GLUTARALDEHYDE REMOVAL FROM PRODUCED WATER USING PHOTOLYSIS AND PHOTOCATALYSIS

Mr. Soklida Hong

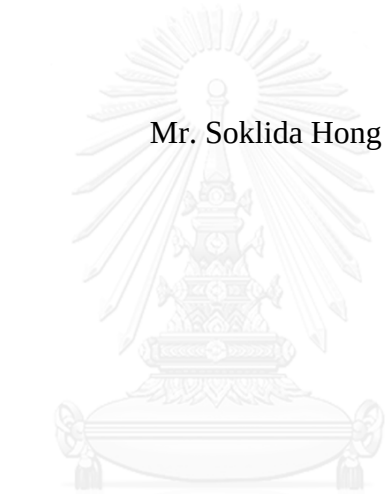

A Thesis Submitted in Partial Fulfillment of the Requirements
for the Degree of Master of Science Program in Environmental Management
(Interdisciplinary Program)
Graduate School
Chulalongkorn University
Academic Year 2016

การกำจัดสารกลูตาราลดีไฮด์ในน้ำผลิตด้วยวิธีโฟโตไลซิสและโฟโตคาตาไลซิส

นายโสลิดา ฮง

วิทยานิพนธ์นี้เป็นส่วนหนึ่งของการศึกษาตามหลักสูตรปริญญาวิทยาศาสตรมหาบัณฑิต
สาขาวิชาการจัดการสิ่งแวดล้อม (สหสาขาวิชา)
บัณฑิตวิทยาลัย จุฬาลงกรณ์มหาวิทยาลัย
ปีการศึกษา 2559

Thesis Title	GLUTARALDEHYDE REMOVAL FROM PRODUCED WATER USING PHOTOLYSIS AND PHOTOCATALYSIS
By	Mr. Soklida Hong
Field of Study	Environmental Management
Thesis Advisor	Professor Eakalak Khan, Ph.D.
Thesis Co-Advisor	Assistant Professor Thunyalux Ratpukdi, Ph.D.

Accepted by the Graduate School, Chulalongkorn University in Partial Fulfillment of the Requirements for the Master's Degree

.....Dean of the Graduate School
(Associate Professor Sunait Chutintaranond, Ph.D.)

THESIS COMMITTEE

.....Chairman
(Associate Professor Srilert Chotpantarat, Ph.D.)
.....Thesis Advisor
(Professor Eakalak Khan, Ph.D.)
.....Thesis Co-Advisor
(Assistant Professor Thunyalux Ratpukdi, Ph.D.)
.....Examiner
(Assistant Professor On-anong Larpparisudthi, Ph.D.)
.....External Examiner
(Assistant Professor Bunyarit Panyapinyopol, Ph.D.)

โสลิดา ฮง : การกำจัดสารกลูตาราลดีไฮด์ในน้ำผลิตด้วยวิธีโฟโตไลซิสและโฟโตคาตาไลซิส (GLUTARALDEHYDE REMOVAL FROM PRODUCED WATER USING PHOTOLYSIS AND PHOTOCATALYSIS) อ.ที่ปรึกษาวิทยานิพนธ์หลัก: ศ. ดร.เอกลักษณ์ คาน, อ.ที่ปรึกษาวิทยานิพนธ์ร่วม: ผศ. ดร.ธัญลักษณ์ ราษฎร์ภักดี, 83 หน้า.

กลูตาราลดีไฮด์เป็นสารฆ่าเชื้อในน้ำที่ผลิตจากกระบวนการสกัดน้ำมันด้วยวิธี hydraulic fracturing (น้ำผลิต) โดยสารกลูตาราลดีไฮด์นั้นมีความเป็นพิษต่อสิ่งแวดล้อม สุขภาพ และสิ่งมีชีวิตในน้ำ ในงานวิจัยนี้ ได้ศึกษาประสิทธิภาพของโฟโตไลซิส และ โฟโตคาตาไลซิส ในการกำจัดกลูตาดีไฮต์จากน้ำผลิต ผลของโฟโตไลซิสด้วยรังสีอัลตราไวโอเลต (UV) พบว่าประสิทธิภาพของการสกัดกลูตัลดีไฮต์เท่ากับ ร้อยละ 52-85 โฟโตไลซิสของกลูตาดีไฮต์เป็นไปตามจลนพลศาตร์ของปฏิกิริยาอันดับหนึ่งแบบเสมือน ความเข้มของรังสี UV ความเข้มข้นของ NaCl และ พีเอชส่งผลกระทบต่ออัตราการย่อยสลายของของกลูตาดีไอต์ สำหรับโฟโตคาตาไลซิส ซึ่งใช้Ag/AgCl/BiOCl เป็นตัวเร่งปฏิกิริยาและแสงที่ความยาวคลื่น 419 นาโนเมตร พบว่า ณ กลูตาดีไฮต์ความเข้มข้น 0.1 mmol NaCl 200 g/L และ พีเอช 7 มีประสิทธิภาพร้อยละ 90 เวลา 75 นาที (Ag/AgCl/BiOCl 5 g/L) อัตราการกำจัดกลูตาราลดีไฮด์มีค่าเพิ่มขึ้น เมื่อพีเอชเพิ่มขึ้น แต่มีค่าลดลงลดลงเมื่อความเข้มข้นNaCl และความเข้มข้นกลูตาราลดีไฮด์เพิ่มขึ้น การกำจัดกลูตาราลดีไฮด์โดยใช้แสงธรรมชาติ ได้ผลดีกว่าแสงที่ความถี่ 419 นาโนเมตรเล็กน้อย

การศึกษานี้ให้ประโยชน์กำจัดน้ำผลิตที่ปนเปื้อนสารกลูตาราลดีไฮด์ โดยสามารถนำน้ำผลิตมาบำบัดต่อด้วยกระบวนการชิวภาพเพื่อให้สามารถนำกลับมาใช้ใหม่หรือทำให้น้ำทิ้งมีความเป็นเป็นพิษลดลง นอกจากนี้งานวิจัยนี้ยังให้แนวทางที่มีประสิทธิภาพในการบำบัดสารฆ่าเชื้อในน้ำผลิตด้วย

สาขาวิชา การจัดการสิ่งแวดล้อม ลายมือชื่อนิสิต .....

ปีการศึกษา 2559 ลายมือชื่อ อ.ที่ปรึกษาหลัก .....

ลายมือชื่อ อ.ที่ปรึกษาร่วม .....

5687657720 : MAJOR ENVIRONMENTAL MANAGEMENT
KEYWORDS: HYDRAULIC FRACTURING, PRODUCED WATER, GLUTARALDEHYDE, PHOTOLYSIS, PHOTOCATALYSIS

SOKLIDA HONG: GLUTARALDEHYDE REMOVAL FROM PRODUCED WATER USING PHOTOLYSIS AND PHOTOCATALYSIS. ADVISOR: PROF. EAKALAK KHAN, Ph.D., CO-ADVISOR: ASST. PROF. THUNYALUX RATPUKDI, Ph.D., 83 pp.

Glutaraldehyde (GA) has been used extensively as a biocide in hydraulic fracturing fluids leading to the contamination of the compound in produced water. In this study, the performances of photolysis and photocatalysis for removal of GA in synthetic produced water were investigated. Photolysis of GA was performed under ultraviolet (UV). GA can be photolyzed by UV at all studied conditions with the removal ranging from 52 to 85% within one hour irradiation. Photolysis of GA followed pseudo-first order kinetics. The degradation rate of GA increased with increasing incident light intensity and decreasing pH. Increasing initial GA concentration resulted in decreasing rate of GA degradation. Photocatalysis of GA used Ag/AgCl/BiOCl as a photocatalyst. Visible light bulbs emitting light at 419 nm were used for photocatalysis. Removal of GA at 0.1 mM in 200 g/L NaCl solution at pH 7 was 90% after 75 min irradiation using 5 g/L of the photocatalyst. The removal rate of GA markedly increased with increasing pH (5-9) and photocatalyst loading (2-8 g/L), and under 350 nm UV (compared to visible light). The removal rate of GA substantially decreased at higher NaCl and GA concentrations. The removal of GA under natural sunlight was slightly better than that under 419 nm. This study helps in addressing an obstacle associated with produced water treatment and disposal. After removing GA from produced waters, biological treatment, which is economical, will become a viable option for treatment of the waters for potential hydraulic fracturing reuse, or will make the waters less harmful after disposal. The work also provides an effective treatment scheme for a common biocide in produced water.

Field of Study:	Environmental Management	Student's Signature	.....
		Advisor's Signature	.....
Academic Year:	2016	Co-Advisor's Signature	.....

ACKNOWLEDGEMENTS

I would like to express my deepest gratitude to my advisor Dr. Eakalak Khan for all of his guidance, encouragement, support and patience that he offered throughout my study at Chulalongkorn University (CU) and North Dakota State University (NDSU). I would like to extend my thankfulness to Dr. Thunylux Ratpukdi my co-advisor at CU and Dr. Jayaraman Sivaguru my co-advisor at NDSU for their support, valuable comments and advices.

I also would like to thank my committee members Dr. Srilert Chotpantarat, Dr. On-anong Larpparisudthi and Dr. Bunyarit Panyapinyopolo for providing constructive comments during my defense.

I would like to thank ASEAN Scholarship Program at Chulalongkorn University for financial support for my study at CU and North Dakota Water Resources Research Institute (NDWRRI) Fellowship program for funding my research.

I wish to thank my friends at CU: Phacharapol Induvesa, Jittrapa Mongkolnawarat, Thaksina Poyai, Boonsiri Dandumrongsin, Artid Poonyakun, Doni Marisi Sinaga, and Nattapong Tuntiwiwattanapun and at NDSU: Chaipon Juntawang, Dhriti Roy and Akila Iyer for their help, motivation and their time to share happiness and joy.

To all the accomplishment, I owe it to my parents and my two little sisters who are always there for me.

CONTENTS

Page

Page

LIST OF TABLES

LIST OF FIGURES

LIST OF ABBREVIATIONS

BQ.....1,4-Benzoquinone

CTAC.....Cetyltrimethylammonium chloride

DI .....Deionized

DOM .....Dissolved organic matter

FID .....Flame ionized detector

GA.....Glutaraldehyde

GC.....Gas chromatography

HR.....High resolution

IPA .....Isopropanol

MS.....Mass spectrometry

PFBHA.....O-(2,3,4,5,6-pentafluorobenzyl)-hydroxylamine-HCl

RF.....Response factor

ROS.....Reactive oxygen species

TDS .....Total dissolved solid

TEOA.....Triethanolamine

TOC.....Total organic carbon

VB .....Valence band

BQ.....1,4-Benzoquinone

CTAC.....Cetyltrimethylammonium chloride

DI .....Deionized

DOM .....Dissolved organic matter

FID .....Flame ionized detector

GA.....Glutaraldehyde

GC.....Gas chromatography

HR.....High resolution

IPA.....Isopropanol

MS.....Mass spectrometry

PFBHA.....O-(2,3,4,5,6-pentafluorobenzyl)-hydroxylamine-HCl

RF.....Response factor

ROS.....Reactive oxygen species

TDS.....Total dissolved solid

TEOA.....Triethanolamine

TOC.....Total organic carbon

VB.....Valence band

CHAPTER 1
INTRODUCTION

1.1 Background

In unconventional oil and gas extraction, hydraulic fracturing has been applied to ensure high and prolonged production of oil and gas from low permeability shale deposits. This technology induces cracking network in low-permeability shale to allow trapped oil and/or gas flow to the production wells by injection of hydraulic fracturing fluid at extremely high pressure and flow rate. After hydraulic fracturing process, there are two types of waters discharged from the well along with oil and gas. These waters are flowback water, mostly hydraulic fracturing water, and formation water, naturally occurred shale water. Flowback and formation waters are collectively known as produced water. Hydraulic fracturing fluids are mainly water (98-99%) and proppant (mostly sand, 1-1.9%); however, several chemicals are added to the fluids to increase hydraulic fracturing performance. Among the chemical additives, biocides are one of the most common additives in hydraulic fracturing fluid. After hydraulic fracturing, biocides are also periodically injected to the wellbores. They are used to prevent corrosion to the wells associated with microbial growth.

Biocides are one of the most harmful contaminants in flowback water (King, 2012; PTAC, 2011; Rimassa et al., 2011). Glutaraldehyde (GA), the most common biocide used in hydraulic fracturing fluid, accounts for 80% of all shale fracturing (King, 2012). It is also used regularly to keep the number of bacterial cells low in the production well (Fakhru'l-Razi et al., 2009). GA is classified as a high level disinfectant due to its lethal action against all types of microorganisms (Russell, 1994). Since it is

used extensively by the oil and gas industry, large amounts of produced water containing GA are generated. GA is a harmful chemical to the environment, human and aquatic organisms. It is a very strong irritant that can cause severe injuries to eyes, skin and respiratory tract. In the environment, it is very toxic to aquatic organisms, especially algae, microorganisms, and fresh water fishes (Leung, 2001).

In addition to its toxicity, another obvious issue with GA in produced water is the restriction of biological activities making biological treatment of the produced water a non-viable alternative. In a study of biodegradability of tanning agents, GA at concentrations of 2.5 mg/L inhibited activated sludge process (Sun et al., 2008). Biological treatment (Bioremediation) is the most preferred treatment technology since it is economical and effective against a variety of environmentally harmful chemicals including those in produced water such as gelling agents, surfactants and organic materials. However, GA, the biocide, is the principle compound that limits the application of biological treatment. Thus, removing GA from flowback and produced waters would be beneficial for the environment, and wastewater treatment, recyclability and disposal.

Photolysis has been used to degrade organic contaminants such as pesticides (Burrows et al., 2002) and pharmaceuticals (Yamamoto et al., 2009). Unlike other treatment technologies, photolysis can be used in all media – aqueous, soil and air. All of organic compounds are photodegradable. The technology requires small footprints, and is easy to operate and effective against organic compounds. On the other hand, photocatalysis involves using of photocatalysts that upon irradiating produce reactive species to activate and/or speed up the reaction. Newly developed photocatalysts can be activated by visible light to degrade pollutants that resist to visible light photolysis.

Both photolysis and photocatalysis are attractive candidates for treating GA in produced water.

1.2 Research objectives

This study aims to apply advanced treatment technology which is photodegradation, including photolysis and photocatalysis to remove GA from brine simulating produced water.

The specific objectives of the study are:

- Determine GA removal efficiency and kinetics by photolysis and photocatalysis;
- Investigate the effects of operating conditions on photolysis and photocatalysis of GA; and
- Elucidate removal mechanisms, pathways, intermediates, by-products, end-products of photolysis and photocatalysis of GA.

1.3 Hypothesis

Under UV light at 254 nm, chemical bonds of GA are broken by absorption of the light resulting in formation of a number of photolytic and photocatalytic intermediates and byproducts that have smaller molecules and are more biodegradable and less toxic than GA.

1.4 Scope of study

In photolysis, the effects light intensity, irradiation time, pH and initial GA concentration were investigated. In photocatalysis, a composite of Ag/AgCl/BiOCl was used as a photocatalyst. The effects of photocatalyst loading, pH, light source, NaCl concentration, and initial GA concentration was investigated in photocatalysis. Brine simulating produced water using NaCl as salt was used. It is possible that intermediate

and by-products that have smaller molecules (compared to GA molecules) will be produced by photodegradation. These molecules, which tend to be more biodegradable (more biologically treatable) were identified.

1.5 Anticipated results and benefits

This project helps to address an obstacle associated with produced water treatment and disposal. After removing glutaraldehyde from produced water, biological treatment, which is economical, becomes viable for treatment of the produced water, or it makes the waters less harmful for disposal. The project delivers a cost-effective treatment scheme for the reuse and disposal of the produced water which in turn will benefit the oil and gas production industry in cost saving on fracturing water and the environment in minimizing pollutants discharge. Additionally, water withdrawal from natural reservoirs for hydraulic fracturing process will be alleviated if produced water can be recycled.

CHAPTER 2
LITERATURE REVIEW

2.1 Produced waters

In unconventional oil extraction, hydraulic fracturing technology has been applied to ensure high and prolonged production of gas and/or oil from shale deposits. This technology induces cracking network in low-permeability shale to allow trapped oil and/or gas flow to the production wells. To do so, hydraulic fracturing fluids are injected into to a wellbore at extremely high pressure and flow rate. Hydraulic fracturing fluid, which 98% to 99% of the total volume is water, contains a variety of additives (Table 2.1) that are added to increase the performance of the fluid and to keep the fractures remain open during the production.

Table 2.1. Hydraulic fracturing fluid additives

Additives	Common chemicals	Proportion (v) %	Purposes
Proppant	Sand	1-1.9*	Keeps the fractures open
Acid	HCl	0.150**	Helps dissolve minerals and initiate cracks in the rock
Scale inhibitor	Phosphate esters	0.075**	Prevent mineral scale precipitates in pipe and fractures
Thickeners	Guar gum	0.05**	Thickens the water to suspend the proppant
Biocide	GA	0.005-0.05*	Disinfect bacteria that produce corrosive by-products
Friction reducer	Polyacrylamide	0.03*	Slicks the water to minimize friction
Surfactants	Lauryl sulfate	0.0005-0.002*	Reduce surface tension of the fluid in the formation and improve fluid recovery from well
Corrosion inhibitor	Amines, amides	0.002**	Protect casing from corrosion

Source: *King (2012); **Ferrer and Thurman (2015)

About 10,000 to 30,000 m^3 of fracturing fluid is required for a single well injection (He et al., 2014). However, the range can vary from 4,000 to 50,000 m^3 per well (Cooley et al., 2012). Typically, 10% to 70% of fracturing fluid returns to the surface as flowback water within the first few weeks after completion of hydraulic fracturing, generating a stream of wastewater that requires proper handling and treatment before being reused or discharged to the environment (Lester et al., 2013). Despite the additives found in fracturing fluids, contaminants in flowback water also come from the formation water and dissolution of shale, which are dissolved and suspended salts and metals, dissolved and non-aqueous hydrocarbons, and in some locations, naturally occurring radioactive materials (Murali Mohan et al., 2013).

Flowback and formation waters are collectively known as produced waters. The concentration of total dissolved solid (TDS) in produced water is up to 400,000 mg/L (Clark and Veil, 2009). During the fracturing process, some additives are used up in the well (strong acids, polymer precursors), while others partially react and come back gradually (surfactants, scale inhibitors, solvents, biocides) (King, 2012; Veil, 2010; Vengosh et al., 2014). Selected characteristics of flowback water from the Marcellus shale, Pennsylvania, United States, are shown in Table 2.2.

Currently, discharge of produced water into salt water wells (deep well injection) is the most common practice. However, recently there has been pressure from authorities and public that push the wastewater (produced water) producers to look for sustainable treatment solutions (Lester et al., 2013). High concentrations of TDS (up to 400 g/L) are the main obstacle for reusing it (He et al., 2014; Olsson et al., 2013). Produced water constituents that have significant impacts on environment are TDS, chlorides, surfactants, gelling agents, metals, corrosion inhibitors, friction reducers, and

biocides (PTAC, 2011). Several steps of treatment are needed before produced water can be reused or safely discharged into the environment.

Table 2.2. Selected chemical characteristics of flowback water sampled 5 days after hydraulic fracturing process

Parameters	Range	Median	Units
pH	5.8 – 7.2	6.6	-
Total Alkalinity	48.8 – 327	138	mg/L
Hardness as $CaCO_3$	5,100 – 55,000	17,700	mg/L
Total suspended solids	10.8 – 3,220	99	mg/L
Turbidity	2.3 – 1,540	80	NTU
Cl^-	26,400 – 148,000	41,850	mg/L
Total dissolved solids	38,500 – 238,000	67,300	mg/L
Total Kjeldahl nitrogen	38 – 204	86.1	mg/L
Nitrate-Nitrite	0.1 – 1.2	N/A	mg/L
Chemical oxygen demand	195 – 17,700	4,870	mg/L
Dissolved organic carbon	30.7 – 501	114	mg/L
Sulfate	2.4 – 106	N/A	mg/L

Source: Thomas (2009)

2.2 Glutaraldehyde

2.2.1 Characteristics

GA (or 1,5-pentanedial) is a saturated aliphatic dialdehyde with registered CAS No. 111-30-8. GA, a colorless to pale straw-colored oily liquid substance with pungent odor, is an industrial biocide, used intensively for over 40 years in many industries such as health care, water treatment, pulp and paper, and oil production. In addition, it is used as a reagent for cross-linking proteins, fixing tissue samples, developing X-ray film, and immobilizing enzyme (Kawahara et al., 1992; Kist et al., 2013; Leung, 2001; Migneault et al., 2004; Russell, 1994). These extensive applications of GA are due to its broad spectrum biocidal activities and versatility on different surfaces including rubber and plastic wares, and for being non-corrosive to stainless steel, soft metal and glass (Banner, 1995; Russell, 1994).

GA is a non-oxidized antimicrobial agent; its biocidal action is depending on the cross-linking with amino groups at the microbial cell surface in such a way that cellular permeability is altered. The ability of the cell wall to transport nutrients to cell and to remove waste products from the cell are disabled resulting in cell death (Russell and Chopra, 1996; Simons et al., 2000). It possesses a fatal biocidal activity against all types of microorganisms, bacteria, mycobacteria, spore, fungi, and viruses, and it is classified as a high-level disinfectant (Russell, 1994).

GA is stable at room temperature, pH from acidic to neutral, and to sunlight. It is mainly available in a stable state as acidic (pH 3.0–4.0) aqueous solutions, ranging in concentration from less than 2% to 70% w/v (Migneault et al., 2004). Properties of GA are shown in Table 2.3.

Table 2.3. Physical and chemical properties of glutaraldehyde

Molecular formula	$C_5H_8O_2$
Structural formula	
Molecular weight	100.12 g/mol
Melting point	-14°C
Boiling point	188°C
Density	0.72 g/cm^3
Vapor pressure	0.6 mm Hg at 25°C
Solubility	water, alcohol, benzene, ether
Water Solubility	Miscible
log K_{ow}	-0.18
Henry's law constant	1.1×10^{-7} atm-m^3/mol
Conversion factor	4.1 mg/m^3 per ppm at 25°C

Source: Emmanuel et al. (2005)

2.2.2 Toxicity

There is no evidence of carcinogenic activity of GA; however, it is considered as a toxic compound that can be irritating and corrosive to skin, eyes and respiratory tract. It is required a well precaution protection for those who are working with the

chemical (Takigawa and Endo, 2006). In the environment, GA is believed to have low adsorption on sediment and low tendency to bioaccumulate. Thus, most of the GA that is released to the environment would remain active in aquatic compartment and is an obvious threat to aquatic organisms (Emmanuel et al., 2005; Leung, 2001). GA is slightly toxic to crabs, (LC_{50} for green crab is 465 mg/L) shrimps and sewage microorganisms, and slightly to moderately toxic to fish and Daphnia. Algae is the most sensitive aquatic species to GA with LC_{50} less than 1 mg/L, while the median lethal concentration of GA for other aquatic organisms is around 7 mg/L (Kist et al., 2013; Leung, 2001).

2.3 Overview of GA remediation

There is a limited number of studies on GA removal. Jordan et al. (1996) used $NaHSO_3$ (sodium bisulfite) to chemically deactivate GA. At pH 8, GA readily reacted with $NaHSO_3$ and complete loss of GA was observed at a ratio of $NaHSO_3$ to GA of 2.2:1. The byproducts (GA-bisulfite complexes) had no effect on the growth of sewage microorganisms even at a concentration as high as 1 mM as GA and the acute toxicity to *Daphnia magna* was reduced by 10-fold compared to that of GA alone.

In another study, Kist et al. (2013) attempted to remove GA from hospital wastewater by UV, O_3, and UV/O_3 (photoozonation). Due to its higher removal efficiency, only UV/O_3 was studied in detailed. At pH 7, the removal efficiency of GA by UV/O_3 from wastewater sample was 23.3% for the first 60 min, while the removal of GA in aqueous solutions was up to 72.0-75.0% for the same conditions. The low degradation for the wastewater sample was caused by reactivity between ozone and $^{\bullet}OH$ (from photolysis of O_3) with other organic compounds.

2.4 Remediation with photolysis

Photolysis has been used to degrade organic contaminants such as pesticides (Burrows et al., 2002) and pharmaceuticals (Lin and Reinhard, 2005; Yamamoto et al., 2009). Unlike other treatment technologies, photolysis can be used in all media – aqueous, soil and air. All of organic compounds are photodegradable but the rates differ enormously from compound to compound depending on their chemical bonds and the incident wavelength. Once organic molecules are irradiated, bonds are rarely broken at random, instead the excited molecules undergo fairly selective bond breaking, rearrangement or bimolecular reactions (Kagan, 1993). For reference, a 254 nm wavelength generates enough energy for homolytic cleavage of almost all chemical bonds of organic molecules (Table 2.4). In general, light containing shorter wavelengths is much more destructive than visible light.

Table 2.4. Energies and wavelengths for homolytic fission of typical chemical bonds

Bond	Energy (kcal/mol)	λ (nm)
C=O*	178	160
C=C	160	179
C–H	95-100	286-301
O–H	85-115	249-336
C–C	85	336
C–O	80-100	249-336
C–Cl	60-86	332-477
C–Br	45-70	408-636
O–O	35	817

*only for carbonyl, ester, amide and halide compounds; for C=O (CO_2) = 191 kcal/mol
Source: Kagan (1993)

In aqueous environment, photolysis occurs in two different mechanisms: (i) direct photolysis where the target compound absorbs light by itself, leading to bond cleavage, and (ii) indirect photolysis where a strongly absorbing molecule other than

the pollutant (photosensitizer) absorbs light and initiates a series of reaction that result in the degradation of the pollutant.

2.4.1 Direct photolysis

Direct light absorption by the target chemical will lead it to excited singlet state, which may then undergo intersystem crossing to produce triplet states. Such excited states can undergo, among other processes: (i) homolysis, (ii) heterolysis, or (iii) photoionization (Figure 2.1).

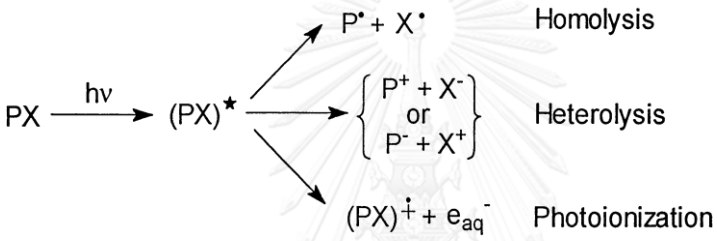

Figure 2.1. Possible chemical events taking place upon direct photolysis (Emília Azenha et al., 2013)

2.4.2 Indirect photolysis

An important benefit of photosensitized photolysis is the possibility of using light of wavelength longer than those corresponding to the absorption characteristic of the pollutant. The most important photosensitizers in aquatic environment are dissolved organic matter (DOM), nitrate, and nitrite. Electronically excited photosensitizers form singlet oxygen ($^1O_2$), $OH^•$, DOM-derived peroxy radicals ($ROO^•$), triplet state DOM (^{3}DOM*), solvated electrons (e^-_{aq}) and other photooxidants that can react with the pollutant (Emília Azenha et al., 2013; Lin and Reinhard, 2005). Following light absorption, the photosensitizer (Sens) can transfer energy from its excited state to the pollutant (equation 2.1), which can then undergo different intermolecular reactions or intermolecular photophysical processes (Figure 2.2).

$$D^* + A \rightarrow D + A^* \qquad \text{(Equation 2.1)}$$

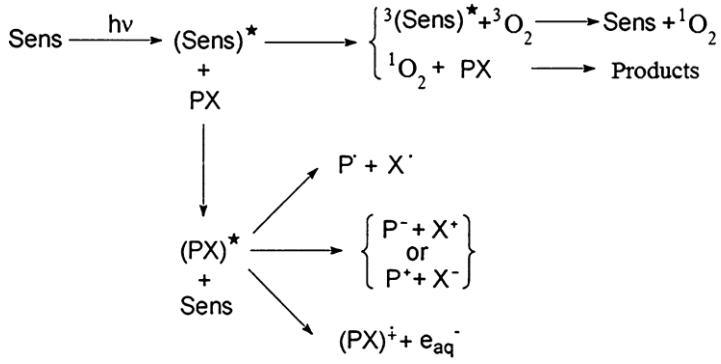

Figure 2.2. Chemical events taking place upon photosensitized photolysis involving energy transfer (Emília Azenha et al., 2013)

2.4.3 Photolysis of aldehydes

Aliphatic aldehydes are known to have absorption bands to UV light in a range of 240-360 nm (Shemesh et al., 2014). In gas state, photolysis of aldehydes undergoes the following reactions:

$$RCHO + h\nu \rightarrow RH + CO \qquad \text{(Equation 2.2)}$$
$$\rightarrow R^{\bullet} + {}^{\bullet}HCO \qquad \text{(Equation 2.3)}$$
$$\rightarrow R_1{=}R_2 + CH_3CHO \qquad \text{(Equation 2.4)}$$
$$\rightarrow RCO + H \qquad \text{(Equation 2.5)}$$

Reaction 2.2 is the molecular fragmentation channel, which yields hydrocarbon and carbon monoxide. Reaction 2.3, Norrish type I reaction, is the radical splitting channel. Two free radicals are formed by this process, the radicals proceed through a variety of secondary reactions to form final products. Reaction 2.4 is called Norrish type II reaction, where the byproducts are alkene and acetaldehyde. This mechanism is only possible for aldehydes larger than butanal. Reaction 2.5 is an H-abstraction process, which is minor in small aldehydes (Haas, 2004; Kagan, 1993; Shemesh et al., 2014).

In term of degradation pathways and byproducts, photolysis of aldehydes in aqueous phase is distinctly different from those in gas phase, presumably owing to the recombination of the produced radicals (Leighton, 1937). The information on photolysis of aldehydes in aqueous phase is very limited. In a study of UV-photolysis of aqueous formaldehyde conducted by Hirshberg and Farkas (1937), they found that some proportion of carboxylic acid was formed, while Pavlovskaya and Telegina (1974) observed that formyl radical ($^{\bullet}HCO$) and glyoxal (combination of two formyl radicals) were formed as the photoproducts of photolysis of aqueous formaldehyde. Hirshberg and Farkas (1937) also found that the removal efficiency of 50 mM of aqueous acetaldehyde was 70% after exposure to UV light for one hour, while the degradation rate of formaldehyde was 40 times slower than that of acetaldehyde.

2.4.4 Remediation with photocatalysis

Photocatalysis is widely referred to the process of using light to activate a substrate (photocatalyst) in order to produce reactive species that could modify and/or facilitate the kinetic of a chemical reaction while the substrate itself remains unconsumed (Banerjee et al., 2014). Photocatalysis has been studied extensively for environmental remediation and energy production since Fujishima and Honda (1972) demonstrated the potential of photoelectrochemical reactivity of TiO_2 to split water.

Figure 2.3 depicts the basic process during photocatalysis. A photocatalyst (usually a semiconductor) absorbs light, where the energy of the incident photons is equal of higher than the band gap of the semiconductor; the absorbed photon induces the excitation of an electron (e^-) from valence band (VB) to the conduction band of the semiconductor leaving a positive electron hole (h^+) on its VB generating high-energy charge carriers (electron-hole pair) in the semiconductor (equation 2.6). The charge

carriers separate and migrate to the surface of the semiconductor where they initiate chemical reactions.

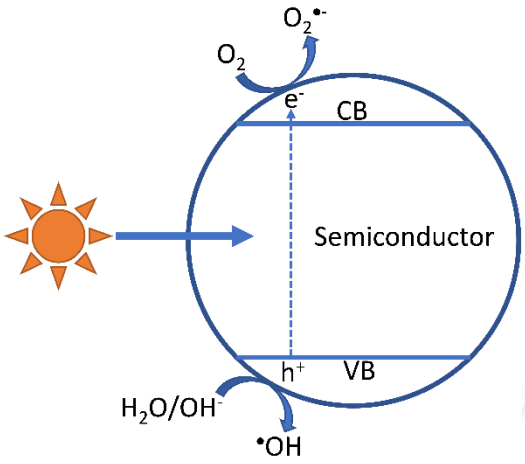

Figure 2.3. Basic process of photocatalysis of a semiconductor

The photoexcited e^- can initiate electrochemical reduction, for example, reducing protons to hydrogen or reducing oxygen to superoxide radical (equation 2.7). The photo-generated h^+ can initiate electrochemical oxidation, for example, oxidizing the molecule water or OH^- absorbed on the surface of the semiconductor to hydroxyl radical (equation 2.8). Both electrochemical oxidation and reduction driven by charge carriers on the surface of the semiconductor generate reactive oxygen species (ROS) that can degrade organic pollutant (equation 2.9). However, the photo-generated charge carriers also undergo recombination that releases energy in a form of heat or luminescence (equation 2.10). This process reduces the overall efficacy of the photocatalysis.

$$\text{semiconductor} + h\nu \rightarrow h^+ + e^- \quad \text{(Equation 2.6)}$$

$$e^- + O_2 \rightarrow O_2^{\bullet-} \quad \text{(Equation 2.7)}$$

$$h^+ + H_2O \rightarrow {}^\bullet OH \quad \text{(Equation 2.8)}$$

$$O_2^{\bullet-}/{}^\bullet OH + \text{organic pollutants} \rightarrow \rightarrow H_2O + CO_2 \quad \text{(Equation 2.9)}$$

$$h^+ + e^- \rightarrow \text{energy} \quad \text{(Equation 2.10)}$$

Titanium dioxide (TiO_2) based photocatalysts are one of the most studied photocatalysts due to their high chemical and physical stability, low toxicity, readily availability, low costs, and excellent photoactivity. Even though with these advantages, TiO_2-based photocatalysts have some drawbacks that limit their uses in environmental and energy applications. The main limitations of TiO_2-based photocatalysts are the rapid recombination of charge carriers resulting in quantum efficiency reduction. In addition, wide band gaps of TiO_2 (3.0 eV for rutile and 3.2 eV for anatase TiO_2) also restrict light absorption to only ultraviolet region ($\lambda < 400$ nm), thus limiting the application of TiO_2-based photocatalysts for solar light harvesting.

In recent years, there has been a particular interest in the development of visible light photocatalysts that can be used to harvest solar energy. Visible light photocatalysis have been considered as one of the most effective strategies to tackle the challenging problems the world facing such as energy shortage, environmental pollution and global warming (Jing et al., 2013; Moniz et al., 2015; Wang et al., 2014).

In environmental applications, visible light photocatalysts have been synthesized and examined their performances on various hazardous pollutants including organic compounds, heavy metals, and pathogens. In a study by Choi et al. (2014), the removal of four pharmaceuticals (Acetaminophen, carbamazepine, cimetidine and propranolol) using Pt doped WO_3 as a photocatalyst under visible light ($\lambda > 400$ nm) has been investigated. At the concentration of 0.5 g/L of photocatalyst and pH 8.0, all four pharmaceuticals (1 μM) were completely removed within 60 min of irradiation in distilled water. However, when tested in secondary effluent from wastewater treatment plant, removal kinetics drastically reduced due to the presence of organic compounds as $^{\bullet}OH$ scavenger in the effluent.

Photocatalysis was applied to reduce toxic and carcinogenic Cr(VI) to Cr(III), which is 100 times less toxic (Wang et al., 2016). AgI/BiOI-Bi_2O_3 was used at a concentration of 1 g/L to remove 4 mg/L of Cr(VI) in DI water at unadjusted pH of 6.08. More than 90% of Cr(VI) was reduced within 90 min irradiation under visible light ($\lambda > 420$ nm) with a first order rate constant of 0.032 min^{-1}. Another application of photocatalysis is for water disinfection. Liu et al. (2016) successfully synthesized highly reactive vertically aligned MoS_2 to inactivate *E. coli* in deionized (DI) water. With a small concentration (1.6 mg/L) of the photocatalyst, more than 99.999% of the bacteria was inactivated within 60 min irradiation under natural sunlight.

CHAPTER 3
UV PHOTOLYSIS OF GLUTARALDEHYDE IN PRODUCED WATER

3.1 Introduction

In unconventional oil and gas extraction, hydraulic fracturing technology has been applied to ensure high and prolonged production of oil and gas from shale deposits. This technology induces cracking network in low-permeability shale to allow trapped oil and/or gas flow to the production wells by injection of hydraulic fracturing fluid at an extremely high pressure and flow rate. Primarily, due to this recently improved technique along with horizontal drilling, unconventional oil and gas production was doubled from 2011 to 2013 in the U.S. (Torres et al., 2016).

Hydraulic fracturing fluid, of which 98% to 99% of the total volume is water, contains a variety of additives that are used to increase the performance of the fluid and to keep the fractures remain open during the production. Typically, hydraulic fracturing requires water ranging from 10,000 to 30,000 m^3 per well (He et al., 2014); however, the range can vary from 4,000 to 50,000 m^3 per well (Cooley et al., 2012). In the first 30 days after the fracturing process is completed, about 10-70% of injected fracturing water returns to the surface (American Petroleum Institute, 2010). This water is called flowback water. Formation water is naturally occurring water in shale. The water that flows to the surface which is flowback water and/or formation water until the end of the life of a well is called produced water. In addition to the additives found in fracturing fluids, contaminants in produced water also come from dissolution of shale, which are dissolved and suspended salts and metals, dissolved and non-aqueous hydrocarbons,

and in some locations, naturally occurring radioactive materials (Murali Mohan et al., 2013). This water tends to have high minerals and hydrocarbons.

According to FracFocus.org, nationwide there are more than 85,000 wells that have been hydraulically fractured. Based on the number of wells and amount of water used in each well, millions of cubic meter of wastewater is inevitably generated. Produced water (oil and gas production wastewater) contains various chemicals that cause significant environmental concerns. Discharging produced water into deep salt water wells is the most common practice; however, recently pressure from authorities and public is pushing the wastewater producers to look for sustainable treatment solutions (Lester et al., 2013). Currently, in Pennsylvania, almost all of the produced water is treated and eventually the treatment could be required nationwide (Rozell and Reaven, 2012).

Biocides are considered one of the most harmful contaminants in produced water (King, 2012; Rimassa et al., 2011). GA, the most common biocide used in hydraulic fracturing fluid, accounts for 80% of all shale fracturing (King, 2012). It is also used periodically to keep the number of bacterial cells low in the production well (Fakhru'l-Razi et al., 2009). GA is classified as a high-level disinfectant due to its lethal action against all types of microorganisms (Russell, 1994). Since it is used extensively by the oil and gas industry, it is very likely that large amounts of produced waters containing GA are being generated (Vengosh et al., 2014). The presence of GA in polymeric forms have been reported in produced water in Colorado (Ferrer and Thurman, 2015). GA a is a harmful chemical to the environment, human and aquatic organisms. It is a very strong irritant that can cause severe injuries to eyes, skin and

respiratory tract. In the environment, it is very toxic to aquatic organisms, especially algae, microorganisms, and freshwater fishes (Leung, 2001).

In addition to its toxicity, the other obvious issue with GA in produced water is the restriction of biological activities making biological treatment a non-viable alternative for them. In a study of biodegradability of tanning agents, GA at concentrations of 2.5 mg/L inhibited activated sludge process (Sun et al., 2008). Biological treatment (Bioremediation) is the most preferred treatment technology since it is economical and effective against a variety of environmentally harmful chemicals including those in produced water such as gelling agents, surfactants, and organic materials. However, GA limits the application of biological treatment. Thus, removing GA from produced water would be beneficial for both the environment and wastewater recyclability and disposal.

There is a limited number of studies on GA removal. Jordan et al. (1996) used $NaHSO_3$ (sodium bisulfite) to chemically deactivate GA. At pH 8, GA readily reacted with $NaHSO_3$ and complete loss of GA was observed at a ratio of $NaHSO_3$ to GA of 2.2:1. The byproducts (GA-bisulfite complexes) had no effect on the growth of sewage microorganisms even at a concentration as high as 1 mM as GA, as well the acute toxicity to *Daphnia magna* was reduced by 10-fold compared to that of GA alone. Kist et al. (2013) attempted to remove GA from hospital wastewater by UV, O_3, and UV/O_3 (photoozonation). Due to its higher removal efficiency, only UV/O_3 was studied in detailed. At pH 7, the removal efficiency of GA by UV/O_3 from wastewater sample was 23.3% for the first 60 min, while the removal of GA in aqueous solutions was up to 72.0-75.0% for the same conditions. The low degradation for the wastewater sample was caused by reactivity between ozone and $^{\bullet}OH$ (from photolysis of O_3) with other

organic compounds. To the best of knowledge, there is no previous study on photolysis of GA in brine nor the photolytic mechanisms and pathway of GA.

This research focused on photolysis of GA in brine solutions simulating pretreated produced waters since this technology has small footprints and is easy to operate and effective against most unsaturated organic compounds. The objectives of the research are (1) to examine the optimal operating conditions such as light intensity and pH for GA photolysis, and (2) to identify the photolytic byproducts of GA and elucidate degradation mechanisms and pathways. Batch experiments of photolysis of GA in synthetic produced water were conducted using a photochamber equipped with UV lamps with primary illumination at 254 nm.

3.2 Methodology

3.2.1 Materials

GA, Grade II in a 25% (w/v) aqueous solution was obtained from Sigma-Aldrich (St Louis, MO, USA). A derivatizing reagent O-(2,3,4,5,6-pentafluorobenzyl)-hydroxylamine-HCl (PFBHA), 99%+ was obtained from Alfa Aesar (Ward Hill, MA, USA). GA and PFBHA were used as received. Analytical grade hexane was purchased from VWR (Radnor, PA, USA). Sodium chloride was purchased from Merck (Darmstadt, Germany) and was baked overnight at 450°C before use. Reverse osmosis DI water was used throughout this research. All other reagents were of analytical grade.

3.2.2 Sample preparation

A stock solution containing 100 mM of GA was prepared by diluting a 25% solution of GA in DI water and stored at 4^{o}C. Synthetic samples were prepared by diluting the stock solution with DI water to obtain desired GA concentrations. NaCl was added to the sample to simulate produced water. Na^{+} and Cl^{-} are the most dominant

constituents and contribute to the majority of total dissolved solids up to 400 g/L in produced water (Clark and Veil, 2009). pH of the synthetic samples was buffered by 10 mM phosphate. pH was adjusted to the final point by either 1 M NaOH or 1 M HCl.

Most experiments were conducted under the following conditions: GA of 0.1 mM, NaCl of 200 g/L, and pH 7. The initial GA concentration of 0.1 mM was chosen based on the potential toxicity and biocidal activities. This level GA inhibits microbial activities (UCC, 1994) and therefore would prohibit the applicability of biological processes for produced water treatment. Moreover, in case of leakage, GA may remain in receiving water to pose adverse effect on aquatic organisms. For example, its lethal concentration (LC_{50}) for algae is less than 0.01 mM (Leung, 2001). The values of NaCl and pH used, are commonly reported in actual produced water (Benko and Drewes, 2008; Clark and Veil, 2009; Gregory et al., 2011). To examine the effects of GA initial concentration, salt concentration, and pH on photolysis performance, the following conditions were experimented: GA concentrations of 0.1, 0.5 and 1 mM; NaCl concentrations of 0, 50, 100, 200 and 300 g/L; and pH 5, 7, and 9. For GA degradation mechanism investigation, isopropyl alcohol (IPA) was added to the sample at 1% (v/v) to quench $^{\bullet}OH$ whereas NaN_3 was added to the sample at 10 mM to quench $^1O_2$. The synthetic samples were prepared fresh daily.

3.2.3 Photoreaction

Photodegradation was conducted in a Rayonet RPR-200 photochamber. The chamber was able to accommodate up to 16 lamps (RPR-2537A). While most of the experiments were conducted with 16 lamps with primary illumination at 254 nm, the effect of light intensity was experimented by controlling the number of lamps installed in the chamber (8, 12 and 16). Based on information from the manufacturer, each lamp

is 14 W in power. Photon irradiance at different light intensities was measured by actinometry (for details see Supplementary Information). One to six cylindrical quartz test tubes (35-mL, Quartz Scientific, Fairport, OH) holding about 25 mL of sample per tube were placed vertically on a merry-go-round, which rotated at 5 rpm in the middle of the reactor. Irradiation was conducted for 60 min with 2-mL sampling for every 10 min using a pipettor. The temperature in the chamber during the experiment was controlled to no more than 40^{o}C during operation by a cooling fan under the chamber. Each photolytic experiment was carried out in triplicate.

3.2.4 GA quantification

GA was derivatized with PFBHA, which reacts with the carbonyl groups of GA to form GA-oxime. The derivative procedure is as follows. In a 5-mL polypropylene tube (Eppendorf, Germany), 2 mL of sample and 0.1 mL of aqueous PFHBA (10 g/L) were placed, mixed and kept in the dark at room temperature for 1 h. After that, 20 µL of 9 M sulfuric acid was added to the mixture followed by 1 mL of hexane containing 1 mg/L of 1,3-dibromopropane, as an internal standard to extract GA-oxime. The mixture was shaken vigorously by hand for 3 minutes and left idle for separation by gravity for another one minute. Finally, the hexane layer was transferred to a 2-mL vial for analysis.

The extract was analyzed by a gas chromatograph-flame ionization detector (GC-FID). A Varian GC-FID (Varian 3900) equipped with HP-5ms, capillary column, (30 m × 0.25 mm with 0.25 µm film thickness) was used. The operating conditions for the GC-FID were as follows: injection volume of 1 µL, He carrier gas constant flow at 1.5 mL/min, injection temperature at 250°C, splitless injection mode with split valve open at 1 min, split flow at 45 mL/min, column temperature at 50°C for 1 min, then

ramping at 4°C/min to 70°C, then at 10°C/min to 210°C, then at 4°C/min to 220°C, then at 40°C/min to 260°C with a 3-min final hold. The total run time was 26.50 min.

The instrument was calibrated daily with five-point calibration (0.001 to 0.1 mM). Standard solutions were prepared fresh from a stock solution in DI water. A calibration curve was constructed based on equation (3.1).

$$RF = \frac{A_{GA}/A_{IS}}{C_{GA}/C_{IS}}$$

(Equation 3.1)

Where: RF = response factor (slope of the calibration curve)
C_{GA} = concentration of GA
C_{IS} = concentration of internal standard (1,3-dibromopropane)
A_{GA} = peak area of GA
A_{IS} = peak area of internal standard

3.2.5 Total organic carbon

Total organic carbon (TOC) was measured using a UV/persulfate oxidation TOC analyzer (Phoenix 8000, Tekmar Dohrmann, OH, USA). To overcome the interference from Cl^-, samples with an initial NaCl concentration of 200 g/L were diluted 10 times with DI water and 40% (w/v) sodium persulfate solution was used to analyze the diluted samples.

3.2.6 Photoproduct analysis

For ease of analysis of photoproducts, GA at 0.2 mM in pure DI water was irradiated for 2 h with 224 W of light intensity (16 lamps). Photoproducts were determined by the High Resolution Mass Spectrometric (HR-MS) method. Mass spectra of unirradiated and irradiated samples were obtained from Synapt G2-Si HDMS with ToF ESI positive mode (Waters, Corporation, Inc). In this method, $^{23}Na^+$ was used as the primary adduct for ionization process. Sample was directly infused into the mass

spectrometer (MS) at a flow rate of 10 μL/min. Before the analysis, the instrument was calibrated using sodium formate as a standard. All m/z values used were within the 5 ppm difference compared to the theoretical masses.

3.2.7 Quantum yield

Quantum yield was determined by mean of ferrioxalate actinometer (Bolton et al., 2011). A ferrioxalate solution for photolytic experiment at 6 mM in 0.1 N H_2SO_4 was prepared as follows. In a 250-mL volumetric flask containing 150 mL DI water, 0.7 mL conc. H_2SO_4 was added slowly followed by 840 mg of $K_2C_2O_4 \cdot H_2O$ and 784.3 mg of $Fe_2(SO_4)_3$ hydrates (Fe^{3+} was at 21.3% determined by UV absorption at 302 nm). The solution was stirred until all the solids dissolved and finally DI water was added to the volume (250 mL). Laboratory lighting was turned off during the preparation of ferrioxalate solution to minimize photolysis of ferrioxalate.

Photolytic reaction of ferrioxalate solution was performed exactly the same as those of GA photolytic experiments. Briefly, a 25-mL of ferrioxalate solution in a quartz test tube was placed in the merry-go-round in the photochamber and the reaction was conducted for 60 s. Different light intensities were used, 224W, 168W and 112W (16, 12 and 8 lamps). The photoreaction experiment was triplicated for each light intensity.

At the end of the photoreaction, 0.5 mL (V_1) of the irradiated sample was added to a 10-mL (V_2) volumetric flask containing 1 mL of 0.1% (w/v) 1,10 phenanthroline and 1 mL of 0.6 M sodium acetate buffer. DI water was added to the final volume (10 mL). The mixture was left for 1 h. The complexation between Fe^{2+} and 1,10 phenanthroline was formed which was then determined based on absorbance at 510 nm. Formed Fe^{2+} was determined by the following equation:

$$\text{moles } Fe^{2+} = \frac{\left(A_{\text{irradiated sample}} - A_{\text{unirradiated sample}}\right) \times V_2 \times V}{\varepsilon_{Fe^{2+}\text{-o-phenanthroline}} \times 1{,}000 \times V_1}$$

(Equation 3.2)

Where: A = absorbance; V_1 = volume of irradiated sample used in complexation (0.5 mL); V_2 = volume of final complexation solution (10 mL); V = volume of irradiated sample (25 mL); and ε = extinction coefficient of Fe^{2+}-*o*-phenanthroline complex (11,100 M^{-1} cm^{-1}).

Photon irradiance, E_p, (einstein cm^{-2} min^{-1}) was determined by the following equation:

$$E_p = \frac{\text{moles } Fe^{2+}}{\Phi_{Fe^{2+}} \times \text{Area} \times t}$$

(Equation 3.3)

Where: $\Phi_{Fe(2+)}$ = 1.25 (mole $einstein^{-1}$) at 254 nm; Area = cross sectional area of the test tube (r = 0.9 cm, area = 2.54 cm^2); and t = irradiated time (1 min).

Finally, the quantum yield of GA was determined by the following equation (Zepp, 1978):

$$\Phi = \frac{k_{obs}}{2.303 E_p \times \varepsilon_{254}}$$

(Equation 3.4)

Where: Φ = quantum yield of GA (mole $einstein^{-1}$); k_{obs} = GA photolysis rate constant (min^{-1}); E_p = photon irradiance (einstein cm^{-2} min^{-1}) obtained from the above ferrioxalate actinometric method, and ε_{254} = extinction coefficient of GA at 254 nm (cm^2 $mole^{-1}$).

3.2.8 Statistical analysis

One-way analysis of variance (ANOVA) test was conducted using Microsoft Windows Excel 2016 to compare the kinetics of GA removal within each treatment (light intensity, pH, GA initial concentration, salt concentration, and quenchers). The significance criterion is $\alpha = 0.05$.

3.3 Results and discussion

3.3.1 Effect of light intensity

After 60 min of irradiation, GA removal by 112, 168 and 224 W (8, 12, 16 lamps) was 57%, 68%, and 80%, respectively suggesting that GA can be photolyzed by UV irradiation (Figure 3.1a). For a control, where the sample was kept in the dark, there was no reduction of GA over the course of 60 min, suggesting that photolysis was responsible for GA degradation. The kinetic model is depicted in Figure 3.1b. It shows that GA photolysis fits well ($R^2 > 0.99$) with pseudo-first order reaction whereas other models (zero and second order) did not show any good regression. GA decomposition rate constant (k_{obs}, min^{-1}) increased about twofold from 0.0137 to 0.0269 min^{-1} with a two-fold increase in light intensity 112 to 224 W. Table 3.1 displays the quantum yield of GA at different light intensity. The quantum yields of GA at the two higher light intensities, were the same while it increased about 20% at the lowest light intensity (112 W) suggesting that photolysis of GA at 112 W was more energy efficient than the higher light intensities. However, in this research the highest light intensity at 224 W, which provided the best removal efficiency (80%) for the same irradiation time, was used in later experiments.

Table 3.1. Quantum yield of GA at different light intensity

Light power	k_{obs} (min^{-1})	ε (cm^2 $mole^{-1}$)	E_p (einstein cm^{-2} min^{-1})	Φ (mole $einstein^{-1}$)
224 W	0.0269	22702	9.3548×10^{-6}	0.0549
168 W	0.0191	22702	6.7001×10^{-6}	0.0545
112 W	0.0137	22702	3.9812×10^{-6}	0.0658

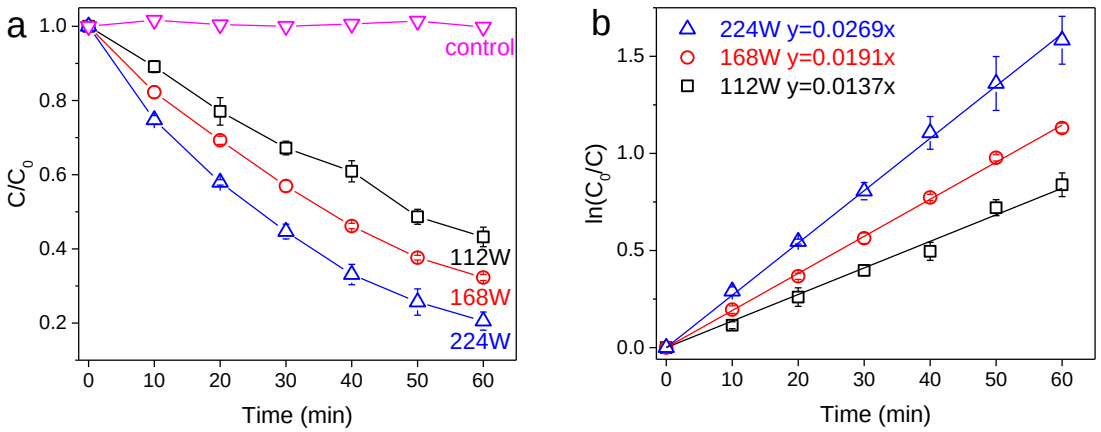

Figure 3.1. Effect of light intensity on GA photolysis (a) removal efficiency and (b) removal rate constant ($[GA]_0$ = 0.1 mM, NaCl = 200 g/L, pH = 7)

3.3.2 Effect of pH

The effect of pH on GA photolysis was studied at pH 5, 7 and 9 using 10 mM phosphate as a buffer. The result indicates that there was an increase of the photodegradation rate constant with decreasing pH. At pH 5, the removal rate was 0.0309 min^{-1} which was insignificantly higher than 0.0269 min^{-1} at pH 7 ($p = 0.054$) but significantly higher than 0.0247 min^{-1} and 9 ($p = 0.017$) see Figure 3.2. A similar result was reported by Kist et al. (2013) that researched on GA removal using O_3/UV, O_3 and UV. They found that under alkaline condition, the efficiency of photolysis of GA under UV was the lowest compared to neutral and acidic conditions. This could be because under acidic conditions, GA is in a more hydrated form which is more susceptible to UV light. Although pH 5 showed better performance of GA photolysis, pH 7 was selected to study in all other experiments because it is the pH commonly reported for produced water (Benko and Drewes, 2008; Clark and Veil, 2009; Gregory et al., 2011).

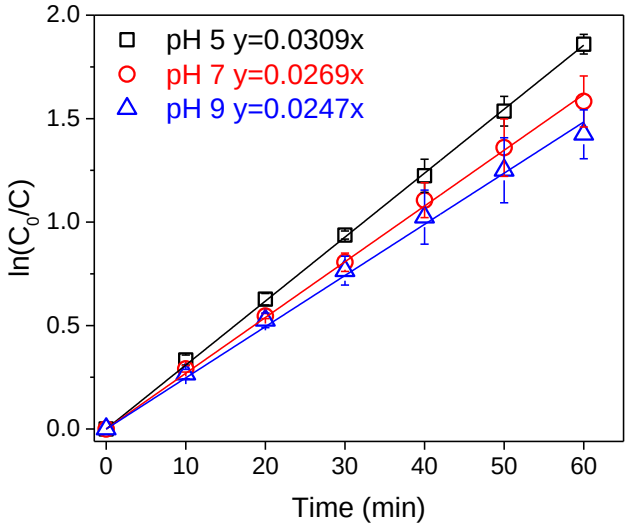

Figure 3.2. Effect of pH on GA photolysis rate ($[GA]_0$ = 0.1 mM, NaCl = 200 g/L, light intensity = 224 W)

3.3.3 Effect of GA initial concentration

Figure 3.3 shows the effect of initial concentration on GA photolysis rate. The photolysis rate constant of GA decreased with increasing initial concentration. About 55% reduction of degradation rate of GA was recorded for a 10-fold increase in initial concentration of GA from 0.1 mM (k_{obs} = 0.0269 min^{-1}) to 1 mM (k_{obs} = 0.0118 min^{-1}). This type of observation had been frequently reported in literature on the photodegradation of organic compounds and was explained by the limit of photon with high concentrations of reactants (Jiao et al., 2008; Prados-Joya et al., 2011).

3.3.4 Effect of salt concentration

The level of salt in produced waters varies greatly with the shale formation and location. It is, therefore, important to investigate the effect of salt concentration on GA photolysis. The result of this research demonstrated that different salt concentrations affected GA degradation rates. At lower salt concentrations, notable retardation of GA degradation rate was observed. As depicted in Figure 3.4 (plots of removal efficiency and rate can be found in Appendix, Figure A1), at 0 g/L of NaCl (no salt), the

photodegradation rate was 0.0247 min^{-1}. At 50 g/L of NaCl, the rate significantly dropped to 0.0161 min^{-1} ($p = 3.18\times10^{-5}$) but increased to 0.0269 min^{-1} at 200 g/L and significantly increased to 0.0281 min^{-1} at 300 g/L of NaCl ($p = 0.006$). It should be noted that the photodegradation rate was better at the two high salt concentrations compared to the no salt case. These trends on photodegradation rate suggest that at low and high salt concentrations different photolysis mechanisms, which are discussed in the following subsection, may govern.

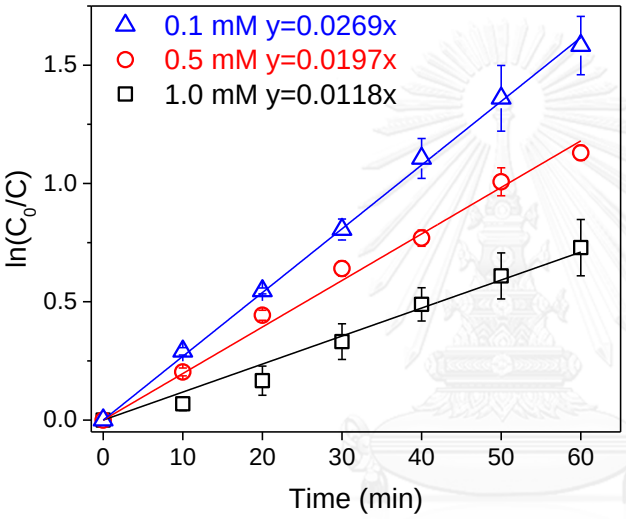

Figure 3.3. Effect of initial concentration on GA photolysis rate (pH = 7, NaCl = 200 g/L, light intensity = 224 W)

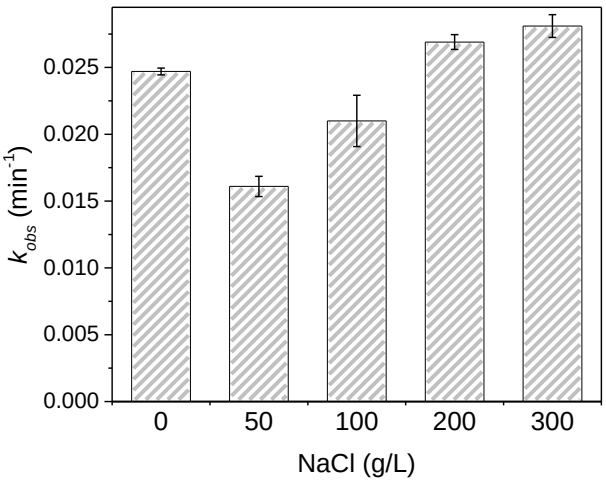

Figure 3.4. Effect of NaCl on the GA photolysis rate ($[GA]_0$ = 0.1 mM, pH = 7, light intensity = 224 W)

3.3.5 Photolytic mechanisms

Figure 3.5 depicts the results from the quenching experiment (plots of removal efficiency and rate can be found at Appendix Figure A2). When isopropyl alcohol (IPA), as •OH scavenger, was added at 1% (v/v) to the sample about 40% reduction in degradation rate of GA (k_{obs} decreased from 0.025 to 0.015 min^{-1}) was observed in the sample without salt compared to 11% reduction (k_{obs} decreased from 0.027 to 0.024 min^{-1}) with salt at 200 g/L. The reduction of GA degradation rate in the presence of IPA suggested the involvement of indirect photolysis of GA via •OH photooxidation. Studies shown that photolysis of carbonyl compounds (aldehydes and ketone) generated organics with peroxyl functional groups including peroxide (Bateman et al., 2011; Faust et al., 1997; Gligorovski et al., 2015; Taraborrelli et al., 2012; Zhu and Zhu, 2010). It is also possible that during photolysis of GA, peroxide was generated and simultaneously photolyzed to •OH.

Although indirect photolysis of GA via •OH photooxidation in saline sample was much less compared to sample without salt, the total removal rate constant for saline sample was higher than that of sample without salt (0.027 min^{-1} versus 0.025 min^{-1}). As mentioned above, other mechanisms may govern the photodegradation of GA in the present of salt rather than •OH.

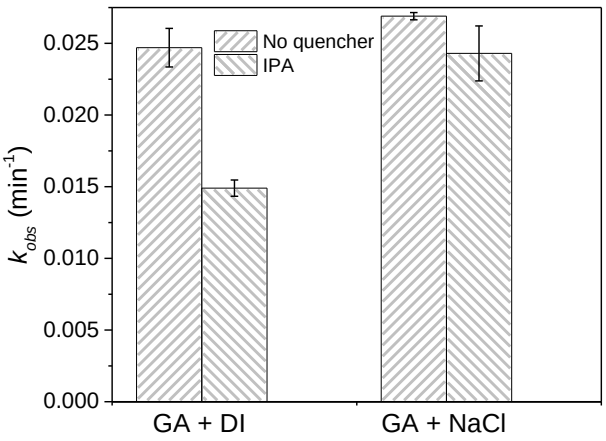

Figure 3.5. Effect of IPA (1% v/v) and NaCl (200 g/L) on the GA photolysis rate ($[GA]_0$ = 0.1 mM, pH = 7, light intensity = 224 W)

In a study of photodegradation of phenicol antibiotics, Ge et al. (2009) found that under UV (wavelength > 200 nm) irradiation, Cl^- in solution promoted singlet oxygen ($^1O_2$) formation which contributed to the photooxidation of phenicol and therefore improved the degradation rate of phenicol compared to photodegradation of phenicol in pure water. They also found that the removal rate constant increased with increasing salt concentration in the range of 0.1 to 1 M. Similar trends were also observed in this research that the increase in salt concentration resulting in higher removal rate of GA (Figure 3.4). However, at low salt concentrations, there was a pronounced decrease in GA removal rate compared to the removal rate of no salt case. This could be because Cl^- is also a scavenger of $^{\bullet}OH$ and at low concentrations of salt and $^1O_2$ formation might be too low to promote indirect photolysis resulting in direct photolysis being the only or main mechanism and consequently lower degradation rate of GA. However, it was not possible to investigate the effect of $^1O_2$ in this research due to the instantaneous reaction between NaN_3 ($^1O_2$ scavenger) and GA under UV.

3.3.6 Photoproducts and photolytic pathways

TOC removal was quite low over the course photolysis, especially in saline sample (See Figure 3.6). This data suggests that complete mineralization was not the main route of GA photolysis and therefore, the majority of organic carbon remained in the solution.

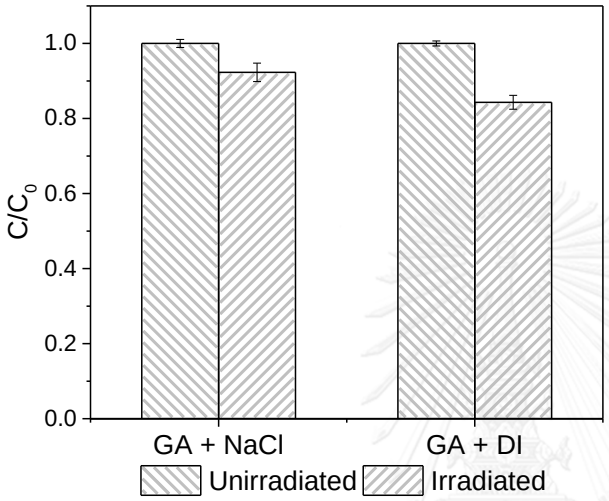

Figure 3.6. Total organic carbon removal of GA in pure DI water and saline sample (NaCl = 200 g/L) after 1 h irradiation ($[GA]_0$ = 0.1 mM, pH = 7, and light intensity = 224 W)

Figure 3.7 summarizes the aqueous chemistry of GA. Aqueous GA is primarily consisted of hydrates, cyclic hemiacetal and its oligomers (Kawahara et al., 1992; Migneault et al., 2004; Whipple and Ruta, 1974). However, Korn et al. (1972) argued that an aqueous solution of 70% GA was primarily composed of structures depicted in Figure 3.7I (15%), Figure 3.7IV and Figure 3.7V (85% for both). Their suggestion agrees with the obtained mass spectrum of GA from HR-MS in this research (Figure 3.8a), which show that structures depicted in Figure 3.7V (n = 2 and 3) and Figure 3.7I were the most predominant species with little amounts of the other structures. It should be noted that peaks at m/z ~223 $[2GA+Na]^+$ and ~323 $[3GA+Na]^+$ were all assigned the free aldehyde form of GA (Figure 3.7I), as it is common for some analytes to have multiple molecules adduct to Na^+.

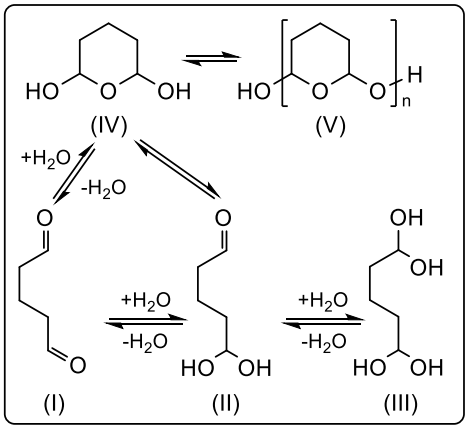

Figure 3.7. Structure of Aqueous GA

Figure 3.8b depicts the mass spectrum of the irradiated sample which contains more than 1,300 peaks. From 150 < m/z < 500, the peak clusters were separated by a repetitive group with m/z ~14. In addition, peaks in this region also exhibited a regular mass difference of m/z ~14, 16 and 18 (equivalence to the exact mass of CH_2, O and H_2O, respectively), suggesting evidence of oligomerization (Kalberer et al., 2004). The oligomerization of GA during photolysis could be from the reaction of the free aldehyde (Figure 3.7I) and the oligomeric hemiacetals (Figure 3.7V) to form irreversible oligomers. Based on the spectrum in Figure 3.8b, this postulation is reasonable due to the majority of the most intense peaks were centralized at m/z 200-300 which corresponded to the dimeric and trimeric photoproducts where dimer and trimer were also the main precursors detected. Similar findings were reported by studies of secondary organic aerosols components as the photoproducts of aldehydes and other organics in cloud droplet (Bateman et al., 2011; Guzmán et al., 2006; Kalberer et al., 2004; Loeffler et al., 2006; Reinhardt et al., 2007; Renard et al., 2014; Tolocka et al., 2004; Walser et al., 2008).

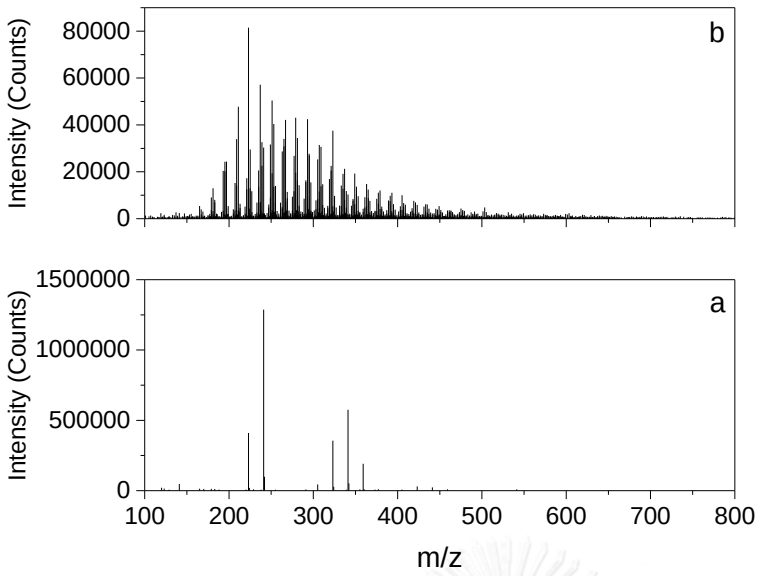

Figure 3.8. ESI positive mode mass spectra of GA (a) before and (b) after irradiation. Initial GA concentration at 0.2 mM in pure DI water was irradiated using 224 W light intensity for 2 h. About 95% of GA were removed after irradiation.

Since the method of GA quantification was also able to detect small carbonyl compounds, trace amounts of formaldehyde, acetaldehyde, acrolein and glyoxal were observed in the chromatogram along with GA during photolysis. Even though they were detected as minor photoproducts, these small aldehydes possess similar chemistry as GA. Therefore, more or less they could also play an important role as the precursors which contributed to wide variety of photoproducts as detect in the mass spectra.

The proposed photolytic pathway of GA is presented in Scheme 1. The main pathway followed the reaction between GA in free aldehyde form with dimer and trimer of its hemiacetal. In this pathway, the photoproducts were oligomers. With the involvement of the generated $^{\bullet}OH/^{1}O_2$, the reaction could be accelerated. In minor pathway, fraction of excited GA in free aldehyde form, underwent both Norrish type I (reaction a1) and Norrish Type II (reaction a4) cleavage (Haas, 2004; Kagan, 1993). Norrish type I cleavage gave formyl radical as one the products. Formyl radical could undergo H-abstraction (reaction a2) from the surrounding compounds to give

formaldehyde, or simply combine with another formyl radical to give glyoxal (Pavlovskaya and Telegina, 1974). In Norrish Type II, GA dissociated at beta carbon to give two free radicals which disproportionated to acrolein and acetaldehyde (Paulson et al., 2006).

Scheme 1. Proposed GA photolysis pathways (with detected photoproducts are in red)

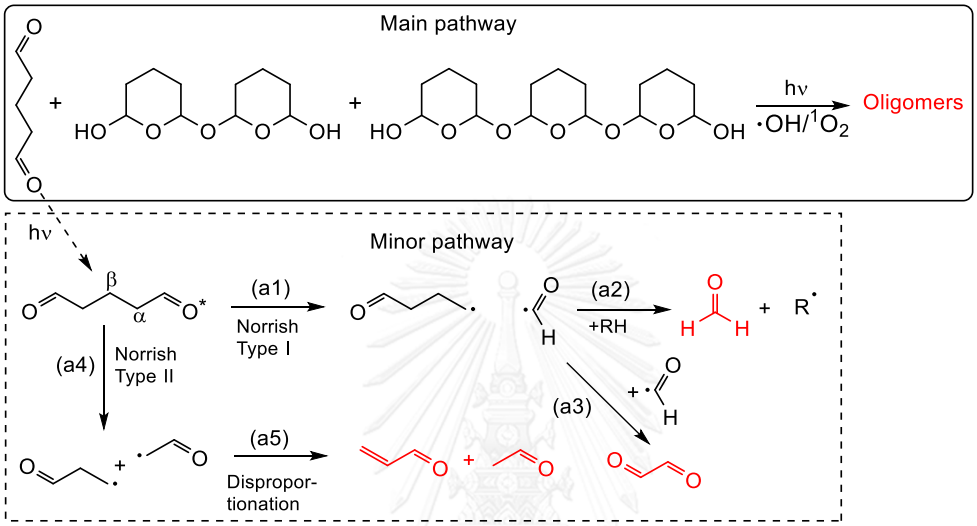

3.4 Summary

GA can be photolyzed by UV at all studied conditions with the removal ranging from 52 to 85% within one hour irradiation. Photolysis of GA followed pseudo-first order kinetics. The degradation rate of GA was substantially affected by light intensity (112-224 W), initial GA concentration (0.1-1 mM) and salt concentrations (0-300 g/L) but minimally influenced by pH (5-9). Photolysis rate constant of GA at 0.1 mM in 200 g/L of salt at pH 7 was 0.0269 min^{-1} with a quantum yield of 0.0549 under 224 W illumination. The degradation rate of GA increased with increasing incident light intensity and decreasing pH. Increasing in initial GA concentration resulted in decreasing degradation rate of GA. At lower salt concentrations, notable retardation of GA degradation rate was observed. Quenching experiments were also conducted; •OH was more dominant in no salt sample as compared to 200 g/L of salt. Oligomers were

identified as the main photolytic byproducts and GA photolytic pathways were proposed. The findings in this research indicate that photolysis is a promising technology in removing GA in flowback and produced waters. GA removal at high salt concentrations, similar to the levels found in produced water, was better than those at zero and low salt concentrations.

CHAPTER 4
PHOTOCATALYSIS OF GLUTARALDEHYDE IN PRODUCED WATER

4.1 Introduction

Chapter 3 describes research on the application of photolysis to degrade GA in brine solutions simulating produced waters under 254 nm UV. GA removal ranging from 52 to 85% could be achieved within one hour of irradiation under the studied conditions such as light intensity (112-224 W), pH (5-9), initial GA concentration (0.1-1 mM) and salt concentration (0-300 g/L). Recently, visible light photocatalysis has drawn considerable interests. The technology has been exploited to harvest natural sunlight for environmental remediation as well as energy production.

Most research in visible light photocatalysis has mainly focused on the fabrication of new photocatalysts. For example, Ag_3PO_4-based photocatalysts had high reactivity toward dye (Yi et al., 2010); however, these photocatalysts are not suitable for a system where Cl^- concentration is high due to reaction of Ag_3PO_4 with Cl^- to form AgCl. Other recently synthesized photocatalysts, AgCl, Ag/AgCl, and BiOCl were studied due to their relatively high reactivity and stability. Although, AgCl, Ag/AgCl (composite of Ag and AgCl), BiOCl are photocatalytically active under visible light, all of them were proven to be less effective than Ag/AgCl/BiOCl composite (Xiong et al., 2011; Ye et al., 2012). As previous studies found that flower-like BiOCl had better performance compared to its flake sheet counterpart (Chen et al., 2013; Chen et al., 2012; Cheng et al., 2013), the performance of the composite photocatalyst can be improved by using flower-like BiOCl. As chloridated compounds, AgCl and BiOCl

would be chemically inert to Cl^- making Ag/AgCl/BiOCl suitable for use in produced water where Cl^- is the predominant anions found.

In this research, Ag/AgCl/BiOCl photocatalyst was synthesized based on flower-like BiOCl and tested for the photocatalytic degradation of GA in brine solutions simulating produced waters. The objectives of the research were (1) to examine the effects of operating conditions such as photocatalyst loading, pH, level of NaCl and initial GA concentration on GA photocatalysis under visible light, (2) to test the performance of GA photocatalysis under UV and natural sunlight irradiations and (3) to identify the photocatalytic mechanisms.

4.2 Methodology

4.2.1 Materials

Glutaraldehyde, Grade II in a 25% (w/v) aqueous solution, $Bi(NO_3)_3 \cdot 5H_2O$, $AgNO_3$, cetyltrimethylammonium chloride (CTAC), 1,4-benzoquinone (BQ), triethanolamine (TEOA), were obtained from Sigma-Aldrich (St Louis, MO, USA). A derivatizing reagent PFBHA, 99%+ was obtained from Alfa Aesar (Ward Hill, MA, USA). GA and PFBHA were used as received without further purification. Analytical grade hexane and isopropanol (IPA) were purchased from VWR (Radnor, PA, USA). Sodium chloride was purchased from Merck (Darmstadt, Germany) and was baked overnight at 450°C before use. Reverse osmosis DI water, was used throughout the research. All other reagents were of analytical grade.

4.2.2 Ag/AgCl/BiOCl synthesis and characterization

The preparation procedure for Ag/AgCl/BiOCl photocatalyst is as follows. A solution of CTAC was prepared beforehand by dissolving 3.2 g of CTAC in 15 mL of DI water. In a 125-mL flask, 30 mL of DI water, 15 mL of glacial acetic acid and 4.85

g of $Bi(NO_3)_3 \cdot 5H_2O$ were placed and stirred until the solution became clear and transparent. The clear solution was then quickly added to the CTAC solution to form microsphere BiOCl particles (Gnayem and Sasson, 2013). The mixture, noted as solution A, was stirred for another hour. Meanwhile, 0.850 g of $AgNO_3$ was dissolved in 940 mL of DI water in a 1-L flask. Then, solution A was added to the aqueous $AgNO_3$ solution to form AgCl/BiOCl and the suspension was stirred for 6 h. The precipitate was collected by filtration through a glass fiber filter (Whatman GF/C, 1.2 μm pore size, also used for all other filtrations in this research) then redispersed in 1 L of DI water before being irradiated under 419 nm for 1 h to give Ag/AgCl/BiOCl suspension. The obtained particles were collected by filtration and washed thoroughly five times with ethanol and five more times with DI water; each washing step was followed by filtration. Finally, the washed Ag/AgCl/BiOCl was dried at 80°C for 8 h to produce a final photocatalyst which was subject to the following characterizations. X-ray diffraction (XRD) was performed on a Philips X'Pert MPD system with Cu Kα radiation (45 kV). Ultraviolet-visible diffuse reflectance spectrum (UV-Vis DRS) was obtained using a Cary 300 UV-Vis spectrophotometer equipped with an Agilent DRA-CA-30I as an internal solid sample holder. Scanning electron microscopy (SEM) was performed using JEOL JSM-7600F.

4.2.3 Synthetic produced water preparation

A stock solution containing 100 mM of GA was prepared by diluting the acquired 25% solution of GA in DI water and stored at 4°C. Synthetic samples were prepared by diluting the stock solution with DI water to obtain desired GA concentrations. NaCl was added to the sample to simulate produced water. Na^+ and Cl^- are the most dominant constituents and contribute to the majority of total dissolved

solids up to 400 g/L in produced water (Clark and Veil, 2009). pH of the synthetic samples was buffered by 10 mM phosphate. pH was adjusted to the final point by either 1 M NaOH or 1 M HCl. Most experiments were conducted under the following conditions: GA of 0.1 mM, NaCl of 200 g/L, and pH 7. The initial GA concentration of 0.1 mM was chosen based on the potential toxicity and biocidal activities. This level GA inhibits microbial activities (UCC, 1994) and therefore would prohibit the applicability of biological processes for produced water treatment. Moreover, in case of leakage, GA may remain in receiving water to pose adverse effect on aquatic organisms. For example, its 50% lethal concentration (LC_{50}) for algae is less than 0.01 mM (Leung, 2001). The values of NaCl and pH used, are commonly reported in actual produced water (Benko and Drewes, 2008; Clark and Veil, 2009; Gregory et al., 2011). The synthetic samples were prepared fresh daily.

4.2.4 Photocatalytic experiment

In a 35-mL test tube, 30 mL of sample and 150 mg (5 g/L) of photocatalyst (except in the effect of photocatalyst loading experiment, the amount of photocatalyst varied as described below) were placed. The mixture was stirred in the dark for 30 min to reach adsorption-desorption equilibrium. Prior to the photocatalytic reaction, 3 mL of sample was withdrawn for GA quantification of which the concentration was recorded as C_0. Photocatalytic degradation was conducted in a Rayonet RPR-200 photochamber which was equipped, in most of the experiment with 16 RPR-4190A lamps with primary illumination at 419 nm and 224 W in power. In the effect of light source experiment, 16 UV lamps (RPR-3500A) providing 350 nm irradiation were used with the same wattage as 419 nm.

During photocatalytic reaction, a test tube was placed and stirred in the middle of the chamber. Aliquot of 3 mL was sampled from the solution every 15 min to study removal efficiency and kinetic of GA photodegradation. The temperature in the chamber during the experiment was controlled to < 40°C during the operation by a cooling fan under the chamber. After the sampling, all aliquots of the suspension were centrifuged at 3,000 rpm for 10 min and the supernatant was used for GA analysis. Photocatalysis under natural sunlight was conducted on a bright sunny day of July 25, 2016 for 2 h from 1:00 PM to 3:00 PM. The location of the experiment was next to Civil and Industrial Engineering Building, North Dakota State University, Fargo, North Dakota, USA. A monthly average of solar energy at the point in July is 7.86 $kWh/m^2/day$ (NASA, 2017).

The effects of photocatalyst loading (2, 5 and 8 g/L), initial GA concentration (0.1, 0.2 and 0.4 mM), salt concentration (0, 100, 200, 250 and 300 g/L), and pH (5, 6, 7, 8, and 9), and light source (419 nm, 350 nm and natural sunlight), on photocatalysis performance were examined. For GA photocatalytic degradation mechanism investigation, IPA, BQ, and TEOA were added to the sample at 1 mM to quench $^{\bullet}OH$, $O_2^{\bullet-}$, and h^+ (holes), respectively. Each photocatalytic experiment described above was carried out in triplicate.

4.2.5 GA quantification

Refer to subsection 3.2.4.

4.2.6 Total organic carbon

Refer to subsection 3.2.5.

4.2.7 Statistical analysis

One-way analysis of variance (ANOVA) test was conducted using Microsoft Windows Excel 2016 to compare the kinetics of GA removal within each treatment (photocatalyst dosage, pH, GA initial concentration, salt concentration, light sources, and quenchers). The significance criterion is $\alpha = 0.05$.

4.3 Results and discussion

4.3.1 Characteristics of Ag/AgCl/BiOCl

The crystallinity, morphology and optical property of the prepared phtocatalyst were measured by XRD, SEM, and UV-Vis DRS. The XRD patterns of prepared BiOCl and AgCl, as shown in Figure 4.1a, matched well with the standard patterns of tetragonal BiOCl (JCPDS no. 06-0249) and cubic AgCl (JCPDS no. 06-0480). The diffraction patterns of the BiOCl and AgCl also exhibit high intensity and were without any impurity peak. This observation suggests high phase purity of the sample. However, the diffraction peaks assigned for Ag^0 were low, this could be due to its low content and high dispersity (Chen et al., 2015; Ye et al., 2012). Despite the difficulty in verifying the presence of Ag^0 with the acquired XRD, the change in color of the suspension from white to grayish purple (Figure 4.1b) from partial photolysis of AgCl confirms the formation of Ag^0. UV-Vis DRS of Ag/AgCl/BiOCl (Figure 4.1c) indicates that the grayish purple Ag/AgCl/BiOCl can absorb all spectrum of visible light, which makes it a good photocatalyst for harnessing natural sunlight. From SEM image shown in Figure 4.1d, BiOCl particles were flower-like microspheres with particle sizes ranging 2-5 μm. The spots on the surface of the microspheres were Ag/AgCl.

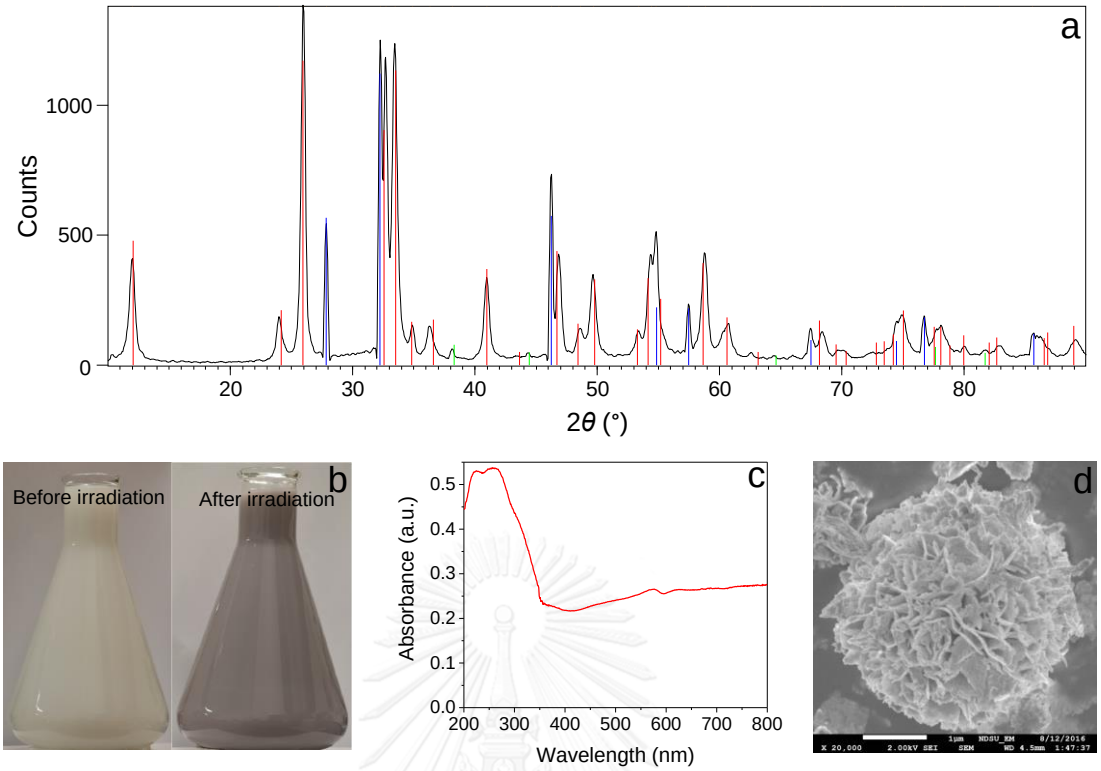

Figure 4.1. a) XRD patterns of the prepared Ag/AgCl/BiOCl photocatalyst. Vertical bars in the middle of the peaks represent the standard diffraction patterns from JCPDS files for BiOCl (no. 06-0249, red), AgCl (no. 06-0480, blue) and Ag (no. 04-0783, green). **b)** Change in color of the prepared Ag/AgCl/BiOCl photocatalyst before and after irradiation. **c)** UV-Vis DRS of the prepared Ag/AgCl/BiOCl photocatalyst. **d)** SEM image of the prepared Ag/AgCl/BiOCl photocatalyst.

4.3.2 Photocatalytic reaction

4.3.2.1 Effect of photocatalyst loading

Figure 4.2 shows the effect of photocatalyst loading on the disappearance of GA over time along with two controls – photolysis (sample was irradiated without adding the photocatalyst) and catalysis (suspension of photocatalyst and sample was kept the dark). There was no sign of GA degradation for both photolysis and catalysis. These results suggest that 419 nm light was not able to induce direct photolysis of GA and there was no reaction taking place between GA and the Ag/AgCl/BiOCl in the dark. The disappearance of GA in the presence of the photocatalyst (2, 5 and 8 g/L) and light therefore suggests that photocatalysis was taking place and served as the principle

process behind this disappearance. At 5 g/L of the photocatalyst, about 95% of GA was removed after 120 min irradiation. However, the photocatalytic degradation of GA occurred mainly in the first 75 min (90% removal). Therefore, the irradiation time of 75 min was selected to study for other experiments including kinetics. At 75 min irradiation, the removal of GA markedly increased when the photocatalyst loading increased from 2 to 5 g/L (43 to 90%) but slightly improved from 5 to 8 g/L (90 to 97%).

The photocatalytic degradation of GA followed pseudo-first order reaction (R^2 > 0.99) whereas other models (zero and second order) did not show any good regression. The rate constants (k_{obs}) of GA photodegradation were 0.0086, 0.0303, and 0.0442 min^{-1} at 2, 5 and 8 g/L of the photocatalyst, respectively. Ag/AgCl/BiOCl have been reported to have high activity against methylene orange and rhodamine B at low photocatalyst loading (0.2-1 g/L) (Xiong et al., 2011; Xu and Lin, 2016; Ye et al., 2012). However, high photocatalyst loadings (2-8 g/L) were used in this research due to prolific water solubility of GA with minimal absorption on the photocatalyst surface, where the photocatalytic reaction occurs more efficiently. TOC removal at 5 g/L of photocatalyst was about 22% at 120 min irradiation. This value was much lower than GA removal (95%) suggesting limited mineralization of GA and formations of intermediate products.

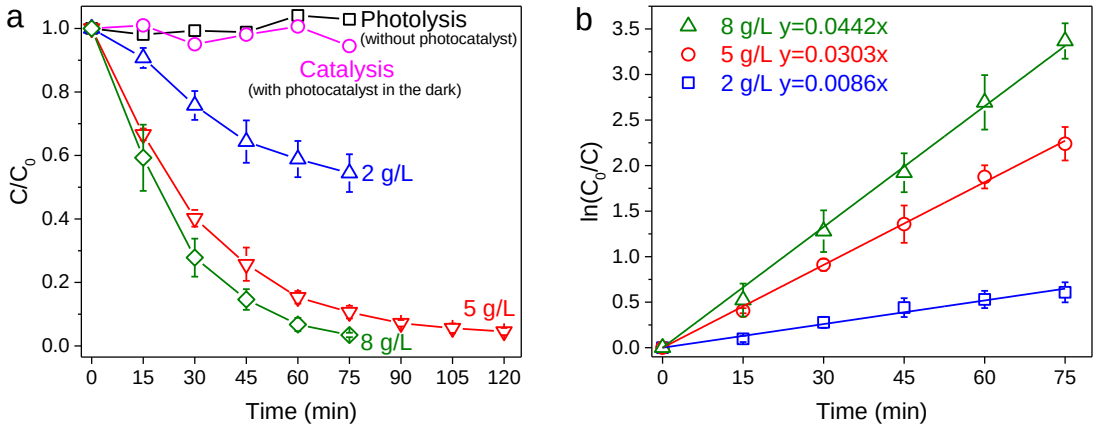

Figure 4.2. Effect of Ag/AgCl/BiOCl loading on **a)** removal efficiency, and **b)** removal rate constant of GA. $[GA]_0$ = 0.1 mM, pH = 7, NaCl = 200 g/L, λ = 419 nm.

4.3.2.2 Effect of pH

pH alters the surface chemistry of the photocatalyst as well the aqueous chemistry of GA. These changes may affect the affinity of GA on the photocatalyst surface, and as a result affecting the decomposition rate of GA. The effect of pH from 5 to 9 (a typical range of pH of produced water) on GA photocatalysis was examined. The rate constant of GA removal increased from 0.0013 to 0.0433 min^{-1} when raising the pH from 5 to 9 (Figure 4.3). Increasing pH 5 to 8 resulted in a significantly higher removal rate of GA ($p = 9\times10^{-7}$) but that was not the case between pH 8 and 9 (p = 0.11). At pH 5, GA photodegradation rate constant was very low (k_{obs} = 0.0013 min^{-1}); however, better result at this pH can be obtained by increasing photocatalyst loading (Figure 4.4). The dependence of GA rate constant on pH of the solution can be explained by the aqueous chemistry of GA itself. Under acidic condition, GA is in a more hydrated form, whereas under alkaline condition aldol condensation of GA is the predominant species. The aldol form of GA is more reactive and may possess stronger affinity to the photocatalyst than the hydrated form of GA. In addition, alkaline condition favors the formation of •OH in the system through reaction of h^+ with more

available OH^-. However, this may not be the case for the observed increase of GA degradation rate in this research. This is because if formed, $^{\bullet}OH$ was primarily consumed by predominant Cl^- in the sample leaving little amount for reaction with GA.

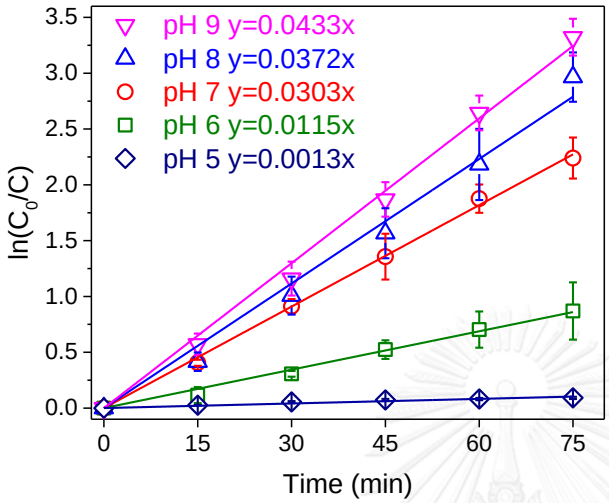

Figure 4.3. Effect of pH on the removal rate constant of GA. Sample pH was buffered by 10 mM phosphate. $[GA]_0$ = 0.1 mM, NaCl = 200 g/L, photocatalyst 5 g/L, λ = 419 nm

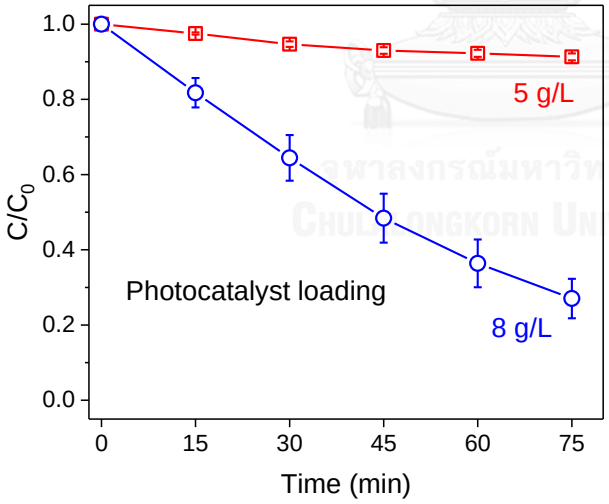

Figure 4.4. Effect of Ag/AgCl/BiOCl loading on removal efficiency of GA at pH 5, $[GA]_0$ = 0.1 mM, NaCl = 200 g/L, λ = 419 nm

4.3.2.3 Effect of NaCl concentration

The level of salt in produced waters varies greatly with the shale formation and location. It is, therefore, important to investigate the effect of salt concentration on GA

photocatalysis. As shown in Figure 4.5, when salt concentration increased, the photodegradation rate of GA decreased. This reduction could be from the changes in ionic strength of the solution. However, only a slight decrease in degradation rate over the range from 0 to 200 g/L of NaCl was observed. At 250 g/L of NaCl, there was about 44% drop of the degradation rate compared to that at 200 g/L NaCl. At 300 g/L of NaCl, the photocatalytic decomposition of GA was completely inhibited. Again, the inhibition of GA removal by this high salt concentration can be overcome by increasing photocatalyst loading (Figure 4.6).

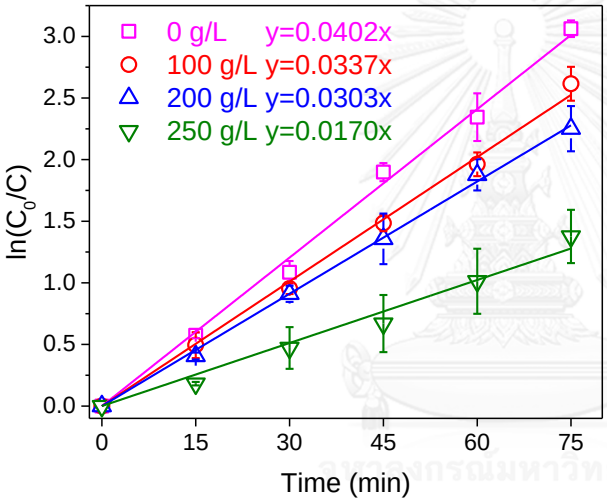

Figure 4.5. Effect of NaCl on removal rate constant of GA. $[GA]_0$ = 0.1 mM, pH = 7, photocatalyst 5 g/L, λ = 419 nm

4.3.2.4 Effect of initial GA concentration

The studied photocatalytic process was able to degrade GA efficiently at 0.1 mM (Figure 4.2a). Two higher initial concentrations of GA at 0.2 mM and 0.4 mM were experimented. There was about 50% reduction of GA photodegradation rate for every two-fold increase in GA initial concentration (Figure 4.7). Upon irradiation, the photocatalyst generated reactive species that reacted with GA (see discussion on degradation mechanisms below). Regardless of the initial GA concentration, the generation of the reactive species was presumably the same. Therefore, when the initial

GA concentration increased, there would be more competition for reactive species to react with GA molecules.

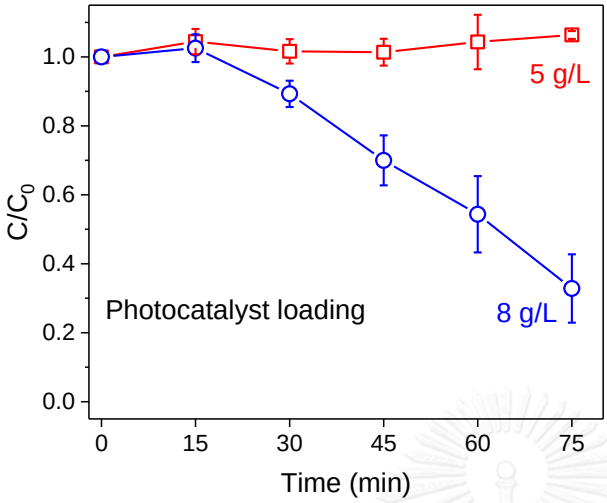

Figure 4.6. Effect of Ag/AgCl/BiOCl loading on removal efficiency of GA at NaCl = 300 g/L, $[GA]_0$ = 0.1 mM, pH = 7, λ = 419 nm

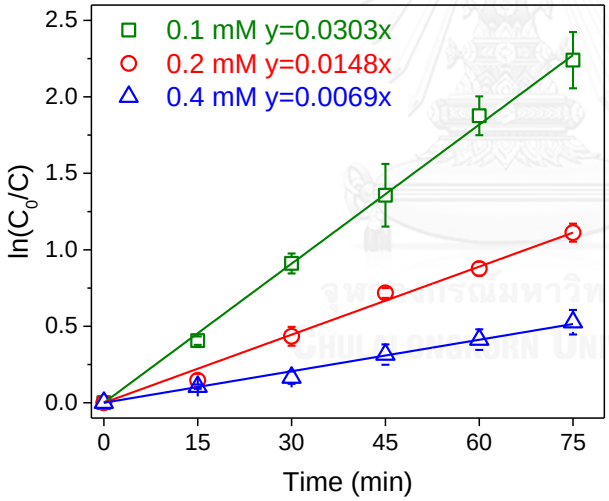

Figure 4.7. Effect of initial concentration on the removal rate constant of GA. NaCl = 200 g/L, pH = 7, photocatalyst 5 g/L, λ = 419 nm

4.3.2.5 Effect of light source

High reactivity under natural sunlight is one of the most desirable functionalities of semiconductor photocatalysts. In this experiment, the performance of the photocatalyst was tested under three different light sources: 419 nm (visible), 350 nm (UV) and natural sunlight (Figure 4.8). Among the three, the removal of GA was

highest under UV with complete removal of GA after 60 min of irradiation. The performance of the photocatalyst under natural sunlight was very similar, except slightly better, to those under 419 nm in terms of GA removal efficiency and kinetics. Direct photolysis (without photocatalyst) of GA under natural sunlight was also conducted. There was no obvious loss of GA observed after 120 min irradiation. The stability of GA against natural sunlight is also reported in literature (Leung, 2001). For the same reason as explained previously, only irradiation time of 75 min was used to study the kinetics. The rate constant of GA removal was the highest under 350 nm irradiation (0.0757 min^{-1}), followed by natural sunlight irradiation (0.0336 min^{-1}) and was the lowest under 419 nm irradiation (0.0303 min^{-1}).

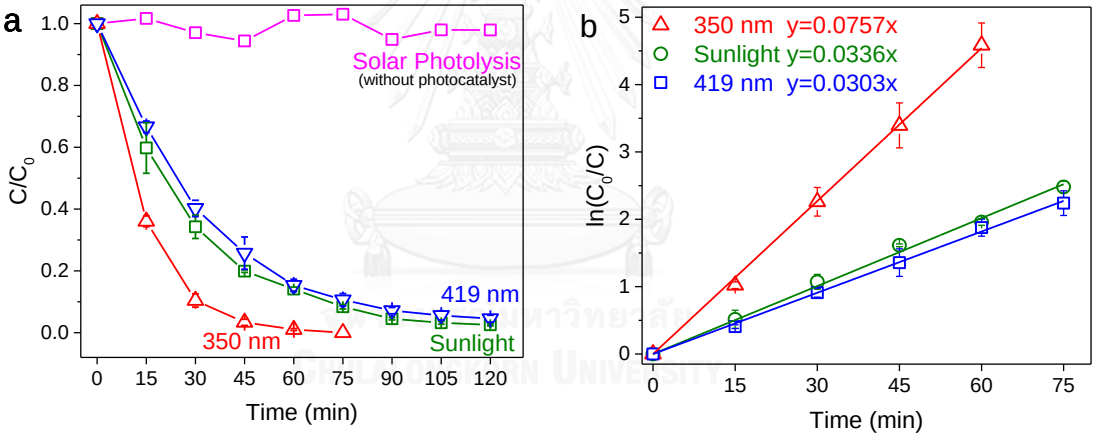

Figure 4.8. Effects of light sources including natural sunlight on removal rate constant of GA. $[GA]_0$ = 0.1 mM, pH = 7, NaCl = 200 g/L, photocatalyst 5 g/L

4.3.2.6 Photocatalytic mechanism

Figure 4.9 shows the effect of quenchers on the removal of GA. IPA, TEOA and BQ at 1 mM were separately used to quenched $^{\bullet}OH$, h^+, and $O_2^{\bullet-}$, respectively. The addition of IPA had a minor effect on GA photodegradation whereas pronounced reduction of GA removal was observed when BQ and TEOA was added, suggesting that $O_2^{\bullet-}$ and h^+ were the main reactive species responsible for the disappearance of GA.

Alongside with direct reaction with contaminants, some generated h^+ was also likely to oxidize Cl^- on the surface of AgCl and BiOCl to give $Cl^\bullet$, which also could oxidize GA (Xiong et al., 2011; Xu and Lin, 2016; Ye et al., 2012). During the reaction, $Cl^\bullet$ was reduced back to Cl^-. Given the wide band gaps, AgCl and BiOCl cannot be activated by visible light (Ye et al., 2012), hence the adsorption of visible light of the photocatalyst was mainly from nano-Ag (n-Ag). Due to its surface plasmon resonance, n-Ag can strongly adsorb visible light and generate charge carriers (e^- and h^+ pairs). Also a dipolar particle, n-Ag can efficiently hinder recombination of the e^- and h^+ making them available for reaction (Wang et al., 2008).

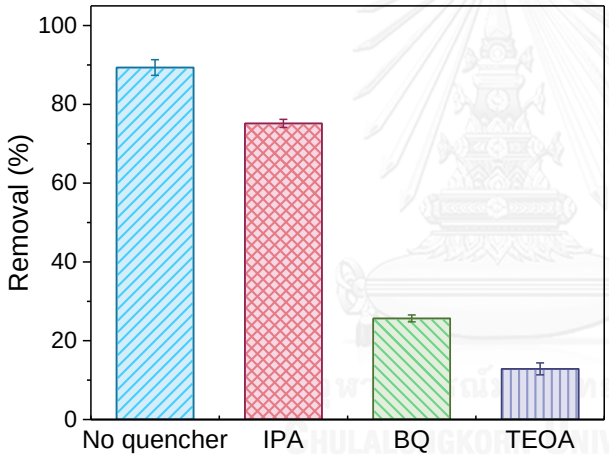

Figure 4.9. Effects of active species quenchers on removal efficiency of GA. $[GA]_0$ = 0.1 mM, pH = 7, NaCl = 200 g/L, photocatalyst = 5 g/L, λ = 419 nm, time = 75 min; [IPA], [BQ], [TEOA] = 1 mM.

A schematic summary of the entire mechanisms is shown in Figure 4.10. Upon irradiation, n-Ag absorbed photon generating e^- and h^+. Then e^- was transferred to conduction band of AgCl and BiOCl. The photogenerated e^- can reduce dissolved O_2 to $O_2^{\bullet-}$ (Wang et al., 2008). On the other hand, the photogenerated h^+ was transferred to the surface of AgCl and BiOCl where it reacted with Cl^- to form $Cl^\bullet$. Together, h^+, $O_2^{\bullet-}$

and $Cl^{\bullet}$ reacted with GA to form intermediates and final products. During reaction, $Cl^{\bullet}$ was reduced back to Cl^{-} again and again.

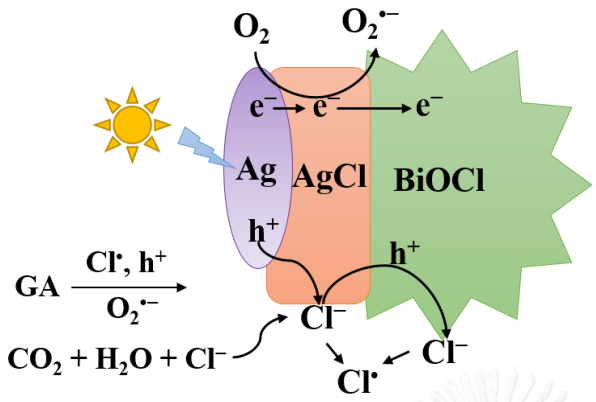

Figure 4.10. Proposed photocatalytic mechanisms of Ag/AgCl/BiOCl on GA

4.4 Summary

Visible light photocatalysis by Ag/AgCl/BiOCl is a promising technology for removing GA in produced water due to its exceptional performance under sunlight irradiation. High photocatalytic activity under sunlight is desirable since it provides free energy for irradiation, more importantly when prolonged irradiation is needed. The results from this research suggested that the performance of GA increased when the concentration of photocatalyst increased, the concentration of NaCl decreased, the pH of the solution increased, the initial concentration of GA decreased, and when UV light was used instead of visible light. Some conditions such as under acidic solutions (pH ≤ 5) or at high salt concentrations (NaCl ≥ 300 g/L), photocatalysis of GA could be hindered. However, this hindrance could be overcome by increasing photocatalyst loading (8 g/L). Experiments on mechanism revealed that the h^{+} and $O_2^{\bullet-}$ as well as $Cl^{\bullet}$, which was widely believed to form during irradiation, were the main reactive species involving in GA photocatalysis. In this research, the ability of Ag/AgCl/BiOCl under

visible light to remove an organic pollutant in brine solutions is proven for the first time.

CHAPTER 5
CONCLUSIONS AND RECOMMENDATIONS FOR FUTURE WORK

5.1 Conclusions

Glutaraldehyde (GA) has been used extensively as a biocide in hydraulic fracturing fluid leading to its presence in oil and gas produced water. In this study, UV photolysis and photocatalysis were used to remove GA from brine solutions simulating produced water.

For photolysis, at studied conditions GA removal efficiency was 52 to 85% within one hour irradiation. Photolysis of GA followed pseudo-first order kinetics. Results also suggest that high salt concentrations (> 200 g/L) increased the removal rat e of GA, making photolysis suitable for GA removal in produced water, which typically contains high salt concentration (up to 400 g/L). Oligomers were identified as the main photolytic byproducts and GA photolytic pathways were proposed.

For photocatalysis, Ag/AgCl/BiOCl was used as a visible light driven photocatalyst for removing GA in produced water. GA could be removed under both simulated visible light and under sunlight irradiation. High photocatalytic activity under sunlight is desirable since it provides free energy for irradiation, more importantly when prolonged irradiation is needed. Under certain conditions such as acidic solutions (pH $\leq$ 5) or high salt concentrations (NaCl $\geq$ 300 g/L), photocatalysis of GA could be hindered. However, this hindrance could be overcome by increasing photocatalyst loading (8 g/L). Experiments on mechanism revealed that the h^+ and $O_2^{\bullet-}$ as well as $Cl^{\bullet}$, which was believed to form during irradiation, were the main reactive species involving

in GA photocatalysis. In this study, the ability of Ag/AgCl/BiOCl under visible light to remove an organic pollutant in brine solutions is proven for the first time.

The findings in this study indicate that photolysis and photocatalysis are promising technologies in removing GA in flowback and produced waters. This study helps in addressing an obstacle associated with produced water treatment and disposal. After removing GA from flowback and produced waters, biological treatment, which is economical, will become a viable option for treatment of the waters for potential hydraulic fracturing reuse, or will make the waters less harmful for disposal. The work also provides an effective treatment scheme for a common biocide in produced water.

5.2 Recommendations for future work

In order to move toward the applications of photolysis and photocatalysis for removal of GA in produced water, the following topics should be investigated.

1. Interferences of other contaminants found in actual produced water such as dissolved salts and other organics (surfactant, guar gum, and dissolved hydrocarbons) on the photolysis and photocatalysis of GA should be examined. These common chemicals may retard (react with ROS or compete for UV) or promote (photosensitizers) the efficiency of photolysis and photocatalysis.
2. Biodegradability and toxicity of GA and its products from both photolysis and photocatalysis should be tested.

Photolysis and photocatalysis of other harmful organics in produced water should be studied in details to demonstrate additional benefits of the processes.

REFERENCES

Banerjee, S., Pillai, S. C., Falaras, P., O'Shea, K. E., Byrne, J. A., and Dionysiou, D. D. (2014). New Insights into the Mechanism of Visible Light Photocatalysis. *The Journal of Physical Chemistry Letters, 5*, 2543-2554. doi:10.1021/jz501030x

The selection of disinfectants for use in food hygiene 315-333 (Springer Netherlands 1995).

Bateman, A. P., Nizkorodov, S. a., Laskin, J., and Laskin, A. (2011). Photolytic processing of secondary organic aerosols dissolved in cloud droplets. *Physical chemistry chemical physics : PCCP, 13*, 12199-12212. doi:10.1039/c1cp20526a

Benko, K. L., and Drewes, J. E. (2008). Produced Water in the Western United States: Geographical Distribution, Occurrence, and Composition. *Environmental Engineering Science, 25*, 239-246. doi:10.1089/ees.2007.0026

Bolton, J. R., Stefan, M. I., Shaw, P. S., and Lykke, K. R. (2011). Determination of the quantum yields of the potassium ferrioxalate and potassium iodide-iodate actinometers and a method for the calibration of radiometer detectors. *Journal of Photochemistry and Photobiology A: Chemistry, 222*, 166-169. doi:10.1016/j.jphotochem.2011.05.017

Reaction pathways and mechanisms of photodegradation of pesticides, 67 71-108 (2002).

Chen, L., Huang, R., Xiong, M., Yuan, Q., He, J., Jia, J., Yao, M.-Y., Luo, S.-L., Au, C.-T., and Yin, S.-F. (2013). Room-Temperature Synthesis of Flower-Like BiOX (X═Cl, Br, I) Hierarchical Structures and Their Visible-Light Photocatalytic Activity. *Inorganic Chemistry, 52*, 11118-11125. doi:10.1021/ic401349j

Chen, L., Yin, S. F., Huang, R., Zhou, Y., Luo, S. L., and Au, C. T. (2012). Facile synthesis of BiOCl nano-flowers of narrow band gap and their visible-light-induced photocatalytic property. *Catalysis Communications, 23*, 54-57. doi:10.1016/j.catcom.2012.03.001

Chen, Y., Fang, J., Lu, S., Wu, Y., Chen, D., Huang, L., Xu, W., Zhu, X., and Fang, Z. (2015). Fabrication, characterization and photocatalytic properties of Ag/AgI/BiOI heteronanostructures supported on rectorite via a cation-exchange method. *Materials Research Bulletin, 64*, 97-105. doi:10.1016/j.materresbull.2014.12.040

Cheng, G., Xiong, J., and Stadler, F. J. (2013). Facile template-free and fast refluxing synthesis of 3D desertrose-like BiOCl nanoarchitectures with superior photocatalytic activity. *New Journal of Chemistry, 37*, 3207. doi:10.1039/c3nj00413a

Choi, J., Lee, H., Choi, Y., Kim, S., Lee, S., Lee, S., Choi, W., and Lee, J. (2014). Heterogeneous photocatalytic treatment of pharmaceutical micropollutants: Effects of wastewater effluent matrix and catalyst modifications. *Applied Catalysis B: Environmental, 147*, 8-16. doi:10.1016/j.apcatb.2013.08.032

Clark, C., and Veil, J. (2009). Produced Water Volumes and Management Practices in the United States. *Argonne National Laboratory Report*, 64. doi:10.2172/1007397

Cooley, H., Donnelly, K., Ross, N., and Luu, P. (2012). *Hydraulic Fracturing and Water Resources : Separating the Frack from the Fiction.* Paper presented at the Pacifc I.

Emília Azenha, M., Romeiro, A., Sarakha, M., Azenha, M. E., and Romeiro, Á. A. (2013). Photodegradation of Pesticides and Photocatalysis in the Treatment of Water and Waste. *Applied Photochemistry*, 247-266. doi:10.1007/978-90-481-3830-2_6

Emmanuel, E., Hanna, K., Bazin, C., Keck, G., Clément, B., and Perrodin, Y. (2005). Fate of glutaraldehyde in hospital wastewater and combined effects of glutaraldehyde and surfactants on aquatic organisms. *Environment International, 31*, 399-406. doi:10.1016/j.envint.2004.08.011

Review of technologies for oil and gas produced water treatment, 170 530-551 (2009).

Faust, B. C., Powell, K., Rao, C. J., and Anastasio, C. (1997). Aqueous-phase photolysis of biacetyl (An α-dicarbonyl compound): A sink for biacetyl, and a source of acetic acid, peroxyacetic acid, hydrogen peroxide, and the highly oxidizing acetylperoxyl radical in aqueous aerosols, fogs, and clouds. *Atmospheric Environment, 31*, 497-510. doi:10.1016/S1352-2310(96)00171-9

Chemical constituents and analytical approaches for hydraulic fracturing waters, 5 18-25 (2015).

Fujishima, a., and Honda, K. (1972). Electrochemical photolysis of water at a semiconductor electrode. *Nature, 238*, 37-38. doi:10.1038/238037a0

Ge, L., Chen, J., Qiao, X., Lin, J., and Cai, X. (2009). Light-source-dependent effects of main water constituents on photodegradation of phenicol antibiotics: Mechanism and kinetics. *Environmental Science and Technology, 43*, 3101-3107. doi:10.1021/es8031727

Gligorovski, S., Strekowski, R., Barbati, S., and Vione, D. (2015). Environmental Implications of Hydroxyl Radicals (•OH). *Chemical Reviews, 115*, 13051-13092. doi:10.1021/cr500310b

Gnayem, H., and Sasson, Y. (2013). Hierarchical nanostructured 3D flowerlike BiOClxBr1-x semiconductors with exceptional visible light photocatalytic activity. *ACS Catalysis, 3*, 186-191. doi:10.1021/cs3005133

Gregory, K. B., Vidic, R. D., and Dzombak, D. A. (2011). Water management challenges associated with the production of shale gas by hydraulic fracturing. *Elements, 7*, 181-186. doi:10.2113/gselements.7.3.181

Haas, Y. (2004). Photochemical alpha-cleavage of ketones: revisiting acetone. *Photochemical & photobiological sciences, 3*, 6-16. doi:10.1039/b307997j

He, C., Wang, X., Liu, W., Barbot, E., and Vidic, R. D. (2014). Microfiltration in recycling of Marcellus Shale flowback water: Solids removal and potential fouling of polymeric microfiltration membranes. *Journal of Membrane Science, 462*, 88-95. doi:10.1016/j.memsci.2014.03.035

Hirshberg, Y., and Farkas, L. (1937). On the Photochemical Decomposition of Aliphatic Aldehydes in Aqueous Solutions. *Journal of the American Chemical Society, 59*, 2453-2457. doi:10.1021/ja01290a105

Institute, A. P. (2010). Water Management Associated with Hydraulic Fracturing. *API Guidance Document, HF2*.

Jiao, S., Zheng, S., Yin, D., Wang, L., and Chen, L. (2008). Aqueous photolysis of tetracycline and toxicity of photolytic products to luminescent bacteria. *Chemosphere, 73*, 377-382. doi:10.1016/j.chemosphere.2008.05.042

Jing, L., Zhou, W., Tian, G., and Fu, H. (2013). Surface tuning for oxide-based nanomaterials as efficient photocatalysts. *Chemical Society reviews, 42*, 9509-9549. doi:10.1039/c3cs60176e

Jordan, S. L., Russo, M. R., Blessing, R. L., and Theis, A. B. (1996). Inactivation of glutaraldehyde by reaction with sodium bisulfite. *Journal of toxicology and environmental health, 47*, 299-309. doi:10.1080/009841096161807

Kagan, J. (1993). Organic Photochemistry: Principles and Applications.

Kalberer, M., Paulsen, D., Sax, M., Steinbacher, M., Dommen, J., Prevot, a. S. H., Fisseha, R., Weingartner, E., Frankevich, V., Zenobi, R., and Baltensperger, U. (2004). Identification of polymers as major components of atmospheric organic aerosols. *Science, 303*, 1659-1662. doi:10.1126/science.1092185

Kawahara, J.-i., Ohmori, T., Ohkubo, T., Hattori, S., and Kawamura, M. (1992). The structure of glutaraldehyde in aqueous solution determined by ultraviolet absorption and light scattering. *Analytical Biochemistry, 201*, 94-98. doi:10.1016/0003-2697(92)90178-A

King, G. E. (2012). Hydraulic Fracturing 101: What Every Representative, Environmentalist, Regulator, Reporter, Investor, University Researcher, Neighbor and Engineer Should Know About Estimating Frac Risk and Improving Frac Performance in Unconventional Gas and Oil Wells. S. *Proceedings of the SPE Hydraulic Fracturing Technology Conference*, 80 pp. doi:10.2118/152596-MS

Kist, L. T., Rosa, E. C., Machado, E. L., Camargo, M. E., and Moro, C. C. (2013). Glutaraldehyde degradation in hospital wastewater by photoozonation. *Environmental Technology, 34*, 2579-2586. doi:10.1037/0022-3514.90.4.644

Korn, A. H., Feairheller, S. H., and Filachoine, E. M. (1972). Glutaraldehyde: Nature of the reagent. *Journal of Molecular Biology, 65*, 525-529. doi:10.1016/0022-2836(72)90206-9

Leighton, P. A. (1937). the Mechanism of Aldehyde and Ketone Photolysis 1. *The Journal of Physical Chemistry, 42*, 749-761. doi:10.1021/j100901a006

Lester, Y., Yacob, T., Morrissey, I., and Linden, K. G. (2013). Can We Treat Hydraulic Fracturing Flowback with a Conventional Biological Process? The Case of Guar Gum. *Environmental Science and Technology Letters, 1*, 133-136. doi:10.1021/ez4000115

Leung, H. W. (2001). Ecotoxicology of glutaraldehyde: review of environmental fate and effects studies. *Ecotoxicology and environmental safety, 49*, 26-39. doi:10.1006/eesa.2000.2031

Lin, A. Y.-C., and Reinhard, M. (2005). Photodegradation of Common Environmental Pharmaceuticals and Estrogens in River Water. *Environmental Toxicology and Chemistry, 24*, 1303. doi:10.1897/04-236R.1

Liu, C., Kong, D., Hsu, P.-C., Yuan, H., Lee, H.-W., Liu, Y., Wang, H., Wang, S., Yan, K., Lin, D., Maraccini, P. A., Parker, K. M., Boehm, A. B., and Cui, Y. (2016). Rapid water disinfection using vertically aligned MoS2 nanofilms and visible light. *Nature Nanotechnology,* 1-8. doi:10.1038/nnano.2016.138

Glutaraldehyde: Behavior in aqueous solution, reaction with proteins, and application to enzyme crosslinking, 37 790-802 (2004).

Moniz, S., Shevlin, S. A., Martin, D., Guo, Z., and Tang, J. (2015). Visible-Light Driven Heterojunction Photocatalysts for Water Splitting– A Critical Review. *Energy Environ. Sci., 8*, 731-759. doi:10.1039/C4EE03271C

Murali Mohan, A., Hartsock, A., Hammack, R. W., Vidic, R. D., and Gregory, K. B. (2013). Microbial communities in flowback water impoundments from hydraulic fracturing for recovery of shale gas. *FEMS Microbiology Ecology, 86*, 567-580. doi:10.1111/1574-6941.12183

NASA. (2017). NASA Surface meteorology and Solar Energy - Available Tables. Retrieved from https://eosweb.larc.nasa.gov/cgi-bin/sse/grid.cgi?&num=084137&lat=46.89&hgt=100&submit=Submit&veg=17&sitelev=&email=skip@larc.nasa.gov&p=grid_id&p=clrskycook&p=swv_dwn&step=2&lon=-96.8

Olsson, O., Weichgrebe, D., and Rosenwinkel, K. H. (2013). Hydraulic fracturing wastewater in Germany: Composition, treatment, concerns. *Environmental Earth Sciences, 70*, 3895-3906. doi:10.1007/s12665-013-2535-4

Paulson, S. E., Liu, D. L., Orzechowska, G. E., Campos, L. M., and Houk, K. N. (2006). Photolysis of heptanal. *Journal of Organic Chemistry, 71*, 6403-6408. doi:10.1021/jo060596u

Pavlovskaya, T. E., and Telegina, T. A. (1974). Photochemical conversions of lower aldehydes in aqueous solutions and in fog. *Origins of Life, 5*, 303-309. doi:10.1007/BF01207632

Prados-Joya, G., Sánchez-Polo, M., Rivera-Utrilla, J., and Ferro-garcía, M. (2011). Photodegradation of the antibiotics nitroimidazoles in aqueous solution by ultraviolet radiation. *Water Research, 45*, 393-403. doi:10.1016/j.watres.2010.08.015

PTAC. (2011). Flowback Reuse Project.

Rimassa, S. M., Howard, P., Mackay, B., Blow, K., and Coffman, N. (2011). Case Study : Evaluation of an Oxidative Biocide During and After a Hydraulic Fracturing Job in the Marcellus Shale. *SPE Int Symposium*, 1 - 10. doi:10.2118/141211-MS

Rozell, D. J., and Reaven, S. J. (2012). Water Pollution Risk Associated with Natural Gas Extraction from the Marcellus Shale. *Risk Analysis, 32*, 1382-1393. doi:10.1111/j.1539-6924.2011.01757.x

Russell, A. D. (1994). Glutaraldehyde: current status and uses. *Infect Control Hosp Epidemiol, 15*(11), 724-733. doi:10.1086/646845

Antiseptics, Disinfectants, and Preservatives: Their Properties, Mechanisms of Action and Uptake into Bacteria 96-149 (1996).

Shemesh, D., Blair, S. L., Nizkorodov, S. A., and Gerber, R. B. (2014). Photochemistry of aldehyde clusters: cross-molecular versus unimolecular reaction dynamics. *Phys Chem Chem Phys, 16*(43), 23861-23868. doi:10.1039/c4cp03130j

Simons, C., Walsh, S. E., Maillard, J. Y., and Russell, A. D. (2000). A NOTE: Ortho-phthalaldehyde: Proposed mechanism of action of a new antimicrobial agent. *Letters in Applied Microbiology, 31*, 299-302. doi:10.1046/j.1472-765X.2000.00817.x

Sun, D., He, Q., Zhang, W., Xin, L., and Shi, B. (2008). Evaluation of environmental impact of typical leather chemicals. Part I: Biodegradability of fatliquors in activated sludge treatment. *Journal of the Society of Leather Technologies and Chemists, 92*, 14-18.

Effects of glutaraldehyde exposure on human health, 48, Japan Society for Occupational Health 75-87 (2006).

Taraborrelli, D., Lawrence, M. G., Crowley, J. N., Dillon, T. J., Gromov, S., Groß, C. B. M., Vereecken, L., and Lelieveld, J. (2012). Hydroxyl radical buffered by isoprene oxidation over tropical forests. *Nature Geoscience, 5*, 300-300. doi:10.1038/ngeo1433

Thomas, H. (2009). Sampling and Analysis of Water Streams Associated with the Development of Marcellus Shale Gas. *Final Report for Marcellus Shale Coalition*, 249 pp.

A review on risk assessment techniques for hydraulic fracturing water and produced water management implemented in onshore unconventional oil and gas production, 539 478-493 (2016).

UCC. (1994). *Bacterial inhibition test results on Ucarcide antimicrobial 250*, South Charleston, WV.

Veil, J. A. (2010). Water Management Technologies Used by Marcellus Shale Gas Producers. *Argonne National Laboratory, Argonne. Prepared for the U.S. Department of Energy, National Energy Technology Laboratory, ANL/EVS/R-10/3.*

A critical review of the risks to water resources from unconventional shale gas development and hydraulic fracturing in the United States, 48, American Chemical Society 8334-8348 (2014).

Wang, H., Zhang, L., Chen, Z., Hu, J., Li, S., Wang, Z., Liu, J., and Wang, X. (2014). Semiconductor heterojunction photocatalysts: design, construction, and photocatalytic performances. *Chemical Society reviews, 43*, 5234-5244. doi:10.1039/c4cs00126e

Wang, P., Huang, B., Qin, X., Zhang, X., Dai, Y., Wei, J., and Whangbo, M.-H. (2008). Ag@AgCl: a highly efficient and stable photocatalyst active under visible light. *Angewandte Chemie (International ed. in English), 47*, 7931-7933. doi:10.1002/anie.200802483

Wang, Q., Shi, X., Liu, E., Crittenden, J. C., Ma, X., Zhang, Y., and Cong, Y. (2016). Facile synthesis of AgI/BiOI-Bi2O3 multi-heterojunctions with high visible light activity for Cr(VI) reduction. *J Hazard Mater, 317*, 8-16. doi:10.1016/j.jhazmat.2016.05.044

Whipple, E. B., and Ruta, M. (1974). Structure of aqueous glutaraldehyde. *The Journal of Organic Chemistry, 39*, 1666-1668. doi:10.1021/jo00925a015

Xiong, W., Zhao, Q., Li, X., and Zhang, D. (2011). One-step synthesis of flower-like Ag/AgCl/BiOCl composite with enhanced visible-light photocatalytic activity. *Catalysis Communications, 16*, 229-233. doi:10.1016/j.catcom.2011.09.027

Xu, Z., and Lin, S.-Y. (2016). Construction of AgCl/Ag/BiOCl of concave-rhombicuboctahedron core-shell hierarchitecture with enhanced photocatalytic activity. *RSC Adv.* doi:10.1039/C6RA14170F

Yamamoto, H., Nakamura, Y., Moriguchi, S., Nakamura, Y., Honda, Y., Tamura, I., Hirata, Y., Hayashi, A., and Sekizawa, J. (2009). Persistence and partitioning

of eight selected pharmaceuticals in the aquatic environment: Laboratory photolysis, biodegradation, and sorption experiments. *Water Research, 43*, 351-362. doi:10.1016/j.watres.2008.10.039

Ye, L., Liu, J., Gong, C., Tian, L., Peng, T., and Zan, L. (2012). Two Different Roles of Metallic Ag on Ag/AgX/BiOX (X = Cl, Br) Visible Light Photocatalysts: Surface Plasmon Resonance and Z-Scheme Bridge. *ACS Catalysis, 2*, 1677-1683. doi:10.1021/cs300213m

Yi, Z., Ye, J., Kikugawa, N., Kako, T., Ouyang, S., Stuart-Williams, H., Yang, H., Cao, J., Luo, W., Li, Z., Liu, Y., and Withers, R. L. (2010). An orthophosphate semiconductor with photooxidation properties under visible-light irradiation. *Nature materials, 9*, 559-564. doi:10.1038/nmat2780

Zhu, C., and Zhu, L. (2010). Photolysis of glycolaldehyde in the 280-340 nm region. *Journal of Physical Chemistry A, 114*, 8384-8390. doi:10.1021/jp104497d

APPENDIX

A1. Photolysis of Glutaraldehyde

A1.1 Glutaraldehyde Photolysis Quantum Yield

Glutaraldehyde (GA) extinction coefficient (Table A1.1) was calculated using Beer-Lambert Law:

$A = \varepsilon \times C \times l$

Where: A = absorbance, C = concentration (M) and l = path length

Table A1 GA Extinction Coefficient λ = 254 nm, l = 1 cm

Abs	C (M)	ε (L/mole cm)
0.057	0.0025	22.8
0.112	0.005	22.4
0.227	0.01	22.7
0.457	0.02	22.85
1.138	0.05	22.76
	Average	22.702
	In cm^2/mole	22702

Table A2 Absorbance of ferrioxalate solution with 1,10 phenanthroline at λ = 510 nm

Sample	Absorbance		
	R1	R2	R3
Unirradiated	0.0260	-	-
Irradiated at 224 W	0.6469	0.7872	0.6257
Irradiated at 168 W	0.4500	0.5542	0.4928
Irradiated at 112 W	0.3156	0.3393	0.2653

A1.2 Figures

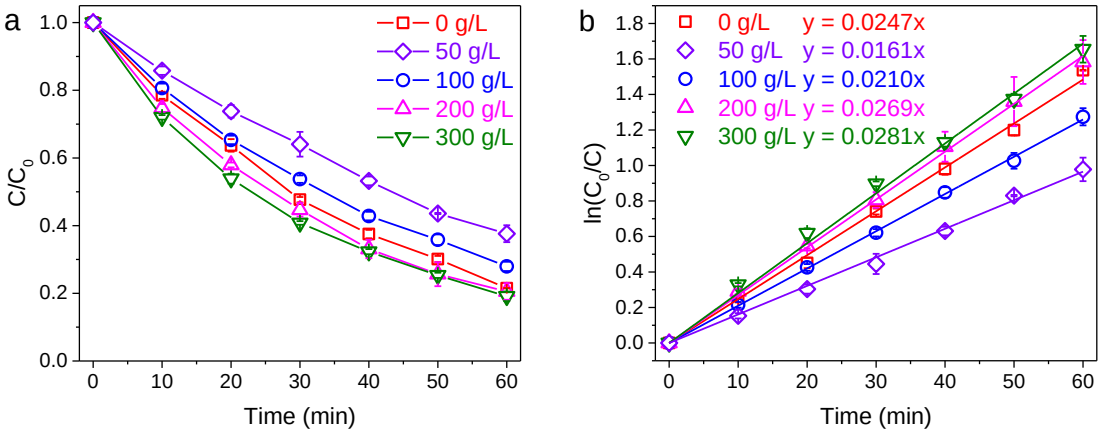

Figure A1. Effect of concentration of NaCl on GA removal (a) efficiency and (b) rate ($[GA]_0$ = 0.1 mM, pH = 7, and light intensity = 224 W)

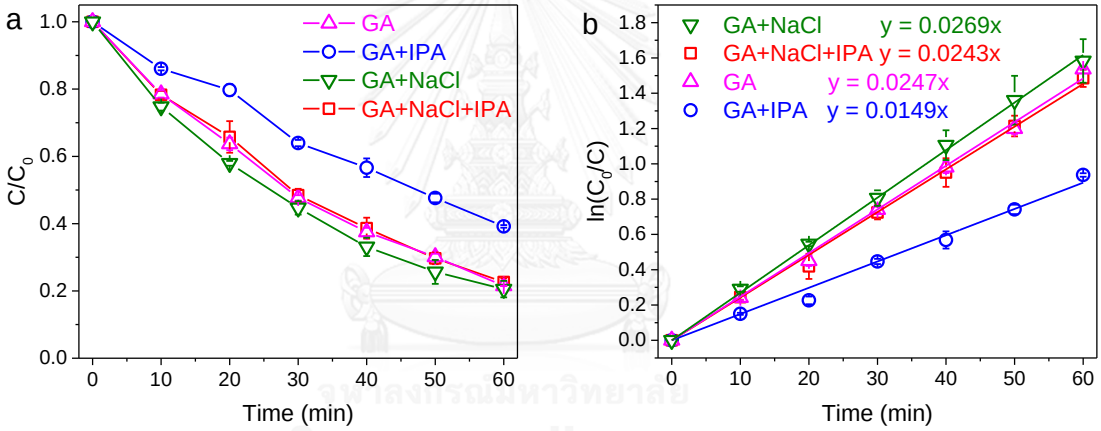

Figure A2. Effect of IPA (1% v/v) on GA removal (a) efficiency and (b) rate ($[GA]_0$ = 0.1 mM, pH = 7, light intensity = 224 W, and NaCl = 200 g/L)

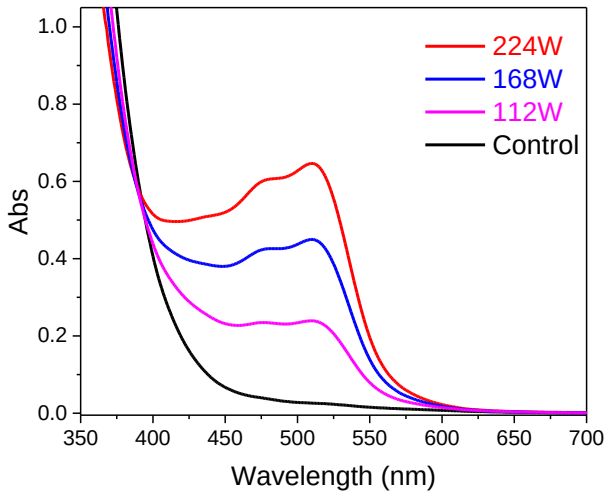

Figure A3. UV-Vis absorption spectra of ferrioxalate samples after 1 min irradiation (254 nm) at different light intensities. Control is unirradiated sample.

Table A3. Concentration of GA (μM) for photolytic experiment on effect of light intensity

GA Std Conc	GC Peak area		RF
	IS	GA	
100	183.2	4375.2	23.88
50	188.8	2281	12.08
20	186.2	888.8	4.77
10	190	514.7	2.70
1	188.6	109	0.57
Blank	175.7	52.8	0.3

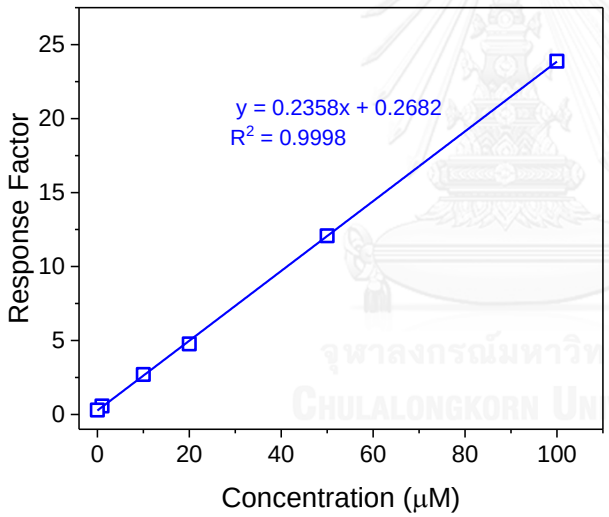

Figure A4. Calibration curve of GA

Table A3. Concentration of GA (μM) for photolytic experiment on effect of light intensity

Sample		Time (min)						
		0	10	20	30	40	50	60
	Control	92.21	93.76	92.64	92.25	92.78	93.53	92.03
112 W	R1	94.88	86.16	77.13	65.73	60.82	48.38	42.77
	R2	96.37	84.44	72.89	63.39	57.81	45.86	39.86
	R3	96.73	86.07	71.87	64.33	56.73	45.84	-
	Avg	95.99	85.56	73.96	64.48	58.45	46.69	41.32
	SD	0.98	0.97	2.79	1.18	2.12	1.46	2.06
168 W	R1	94.06	79.08	66.21	54.99	44.21	35.65	29.52
	R2	95.49	77.50	65.12	52.91	43.67	36.35	31.03
	R3	99.02	80.67	68.59	56.39	45.30	36.57	32.64
	Avg	96.19	79.08	66.64	54.76	44.39	36.19	31.06
	SD	2.55	1.59	1.77	1.75	0.83	0.48	1.56
224 W	R1	95.29	71.05	55.94	42.12	33.64	26.85	21.17
	R2	98.52	74.91	56.43	46.18	33.45	-	21.34
	R3	92.09	67.91	53.24	39.57	27.65	21.32	16.34
	Avg	95.30	71.29	55.20	42.62	31.58	24.09	19.62
	SD	3.22	3.51	1.72	3.33	3.40	3.91	2.84

Table A4. Concentration of GA (μM) for photolytic experiment on effect of pH

Sample		Time (min)						
		0	10	20	30	40	50	60
pH 5	R1	97.06	67.63	52.68	38.84	31.11	22.62	15.64
	R2	94.81	68.58	51.41	36.96	25.97	19.3	13.98
	R3	95.33	69.53	49.31	36.71	27.45	19.93	15.12
	Avg	95.73	68.58	51.13	37.50	28.18	20.62	14.91
	SD	1.18	0.95	1.70	1.16	2.65	1.76	0.85
pH 7	R1	95.29	71.05	55.94	42.12	33.64	26.85	21.17
	R2	98.52	74.91	56.43	46.18	33.45	-	21.34
	R3	92.09	67.91	53.24	39.57	27.65	21.32	16.34
	Avg	95.30	71.29	55.20	42.62	31.58	24.09	19.62
	SD	3.22	3.51	1.72	3.33	3.40	3.91	2.84
pH 9	R1	99.14	74.81	57.04	45.17	33.75	27.05	24.79
	R2	94.09	74.04	57.88	47.21	38.96	31.78	24.68
	R3	94.67	71.85	55.27	41.49	30.6	23.54	19.84
	Avg	95.97	73.57	56.73	44.62	34.44	27.46	23.10
	SD	2.76	1.54	1.33	2.90	4.22	4.14	2.83

Table A5. Concentration of GA (μM) for photolytic experiment on effect of GA initial concentration

Sample		Time (min)						
		0	10	20	30	40	50	60
1000 μM	R1	898.95	811.72	766.29	643.26	569.03	493.35	447.83
	R2	943.32	896.12	747.12	627.19	532.55	461.45	396.55
	R3	927.63	878.76	830.43	717.02	595.31	550.56	490.69
	Avg	923.30	862.20	781.28	662.49	565.63	501.79	445.02
	SD	22.50	44.57	43.63	47.90	31.52	45.15	47.13
500 μM	R1	469.8	390.66	295.08	240.19	214.9	172	148.47
	R2	458.17	369.65	300.14	249.74	206.77	177.06	-
	R3	451.81	365.87	290.53	237.24	217.61	155.14	149.3
	Avg	459.93	375.39	295.25	242.39	213.09	168.07	148.89
	SD	9.12	13.36	4.81	6.53	5.64	11.48	0.59
100 μM	R1	95.29	71.05	55.94	42.12	33.64	26.85	21.17
	R2	98.52	74.91	56.43	46.18	33.45	-	21.34
	R3	92.09	67.91	53.24	39.57	27.65	21.32	16.34
	Avg	95.30	71.29	55.20	42.62	31.58	24.09	19.62
	SD	3.22	3.51	1.72	3.33	3.40	3.91	2.84

Table A6. Concentration of GA (μM) for photolytic experiment on effect of salt concentration

Sample		Time (min)						
		0	10	20	30	40	50	60
NaCl 0	R1	97.18	76.74	62.19	47.18	35.32	28.32	20.89
	R2	93.54	72.34	61.19	43.95	34.98	28.4	20.09
	R3	99.16	78.64	61.21	47.11	38.47	30.65	21.4
	Avg	96.63	75.91	61.53	46.08	36.26	29.12	20.79
	SD	2.85	3.23	0.57	1.84	1.92	1.32	0.66
NaCl 50	R1	103.54	89.76	74.22	62.09	53.65	45.22	36.08
	R2	90.32	76.24	67.95	60.55	48.9	39.49	35.74
	R3	103.74	89.53	77.29	67.59	55.74	45.02	39.85
	Avg	99.20	85.18	73.15	63.41	52.76	43.24	37.22
	SD	7.69	7.74	4.76	3.70	3.51	3.25	2.28
NaCl 100	R1	94.77	77.85	60.85	49.76	39.22	32.39	25.34
	R2	91.38	72.79	60.94	49.94	39.79	34.11	26.9
	R3	96.81	77.65	63.04	52.36	42.18	34.85	26.85
	Avg	94.32	76.10	61.61	50.69	40.40	33.78	26.36
	SD	2.74	2.87	1.24	1.45	1.57	1.26	0.89
NaCl 200	R1	95.29	71.05	55.94	42.12	33.64	26.85	21.17
	R2	98.52	74.91	56.43	46.18	33.45	-	21.34
	R3	92.09	67.91	53.24	39.57	27.65	21.32	16.34
	Avg	95.30	71.29	55.20	42.62	31.58	24.09	19.62
	SD	3.22	3.51	1.72	3.33	3.40	3.91	2.84
NaCl 300	R1	89.65	65.2	48.09	36.43	28.18	22.85	17.52
	R2	92.86	66.28	48.79	37.46	30.35	24.14	18.81
	R3	96.1	69.12	53.28	39.78	31.52	23.52	16.86
	Avg	92.87	66.87	50.05	37.89	30.02	23.50	17.73
	SD	3.23	2.02	2.82	1.72	1.69	0.65	0.99

Table A7. Concentration of GA (μM) for photolytic experiment on photolytic mechanism

Sample		Time (min)						
		0	10	20	30	40	50	60
GA in DI	R1	97.18	76.74	62.19	47.18	35.32	28.32	20.89
	R2	93.54	72.34	61.19	43.95	34.98	28.4	20.09
	R3	99.16	78.64	61.21	47.11	38.47	30.65	21.4
	Avg	96.63	75.91	61.53	46.08	36.26	29.12	20.79
	SD	2.85	3.23	0.57	1.84	1.92	1.32	0.66
GA in DI + IPA	R1	88.2	76.08	70.76	56.8	51.01	42.45	34.65
	R2	88.67	76.61	71.96	57.3	51.95	43.06	35.04
	R3	93.12	79.63	72.45	58.53	49.8	43.02	36.09
	Avg	90.00	77.44	71.72	57.54	50.92	42.84	35.26
	SD	2.72	1.92	0.87	0.89	1.08	0.34	0.74
GA + NaCl	R1	95.29	71.05	55.94	42.12	33.64	26.85	21.17
	R2	98.52	74.91	56.43	46.18	33.45	-	21.34
	R3	92.09	67.91	53.24	39.57	27.65	21.32	16.34
	Avg	95.30	71.29	55.20	42.62	31.58	24.09	19.62
	SD	3.22	3.51	1.72	3.33	3.40	3.91	2.84
GA + NaCl + IPA	R1	92.73	73.07	61.36	45.41	36.77	28.28	21.47
	R2	91.48	70.41	55.84	42.48	32.12	25.31	19.55
	R3	90.55	71.64	63.47	45.28	37.3	28	21.22
	Avg	91.59	71.71	60.22	44.39	35.40	27.20	20.75
	SD	1.09	1.33	3.94	1.66	2.85	1.64	1.04

Table A8. TOC (mg/L) of GA for photocatalytic experiment on photolytic mechanism

Sample		Time (min)	
		0	60
TOC (mg/L) of GA in DI	R1	6.14	5.11
	R2	6.21	5.18
	R3	6.23	5.39
	Avg	6.19	5.23
	SD	0.05	0.15
TOC (mg/L) of GA + NaCl	R1	6.30	5.90
	R2	6.25	5.85
	R3	6.18	5.53
	Avg	6.24	5.76
	SD	0.06	0.20

A1.4 High Resolution Mass Spectra of GA

Table A9. High Resolution Mass Spectra of GA before irradiation

Mass	Intensity	Mass	Intensity
120.0332	20950	355.1721	9541
123.0422	14640	359.1679	191000
129.0387	7339	360.1708	11640
141.0525	47930	373.1832	8148
165.0911	13530	377.1783	10140
170.0595	11990	405.1885	7560
179.0651	12970	423.1993	30100
183.0335	11890	441.209	23670
188.0706	8011	459.2195	9418
220.0859	7767	541.2614	9238
223.0948	409800		
224.0976	20100		
229.0909	9343		
238.0967	7078		
241.1054	1287000		
242.1085	99170		
255.1199	6815		
291.1201	8532		
305.1361	44320		
323.1468	355500		
324.15	27670		
339.1398	6811		
341.1569	575000		
342.1606	52140		

Table A10. High Resolution Mass Spectra of GA after irradiation

Mass	Intensity	Mass	Intensity	Mass	Intensity
119.0859	2355	199.0938	5375	231.1015	2045
137.0963	2732	205.0843	4006	233.0787	2525
141.0533	2450	205.1211	2207	233.1154	6906
147.0808	2257	207.065	3518	235.0949	20590
155.0684	2096	207.1	15210	235.1306	13620
165.0904	5420	209.0792	33940	237.0752	6626
167.069	3949	209.1156	14150	237.11	57160
169.0858	3049	211.058	3260	237.146	7135
177.0896	2035	211.0947	47760	238.1135	3522
179.0696	9065	211.1315	3679	239.0896	32630
179.1063	3572	212.0967	3056	239.1252	22560
181.0486	3167	213.0748	6364	240.0932	2480
181.0844	12960	213.1093	4611	241.0698	2026
183.0635	8041	219.1002	5157	241.1047	30360
183.1004	6979	219.1367	2162	242.1062	2247
185.081	2201	221.0795	12580	245.1144	2409
191.1057	2938	221.1156	17270	247.0957	4804
193.0841	20380	223.0946	81520	247.1306	6043
193.1215	3405	223.1315	11750	249.1104	31660
195.0635	20250	224.0981	4299	249.1461	8962
195.0998	24300	225.0748	12920	250.1132	2490
197.0787	24330	225.1103	29490	251.0901	19420
197.1157	4561	227.0894	11710	251.1256	50410
199.0594	2016	227.1253	2827	251.1622	3596

Table A10. High Resolution Mass Spectra of GA after irradiation

Mass	Intensity	Mass	Intensity	Mass	Intensity
252.1276	3224	269.1003	11400	289.1411	8557
253.0692	2604	269.136	8693	289.1772	2000
253.105	40420	271.1187	3420	291.1218	16350
253.1408	13650	273.108	2345	291.1559	15650
254.108	2978	275.1256	9378	292.1258	2257
255.0855	7096	275.1619	3209	293.1003	6895
255.1202	13970	277.1057	11720	293.1365	42470
257.101	3273	277.1411	26820	293.1731	9092
259.1314	2192	277.1777	2373	294.1395	4102
261.1099	6844	278.1432	2310	295.1172	27690
261.1461	4777	279.084	2559	295.1512	26880
263.0883	4114	279.1212	43050	295.1897	2101
263.1259	28670	279.1561	19610	296.1199	2899
263.1622	4882	280.1244	3580	296.1529	2296
264.1273	2253	281.1009	16320	297.0947	3043
265.1064	34040	281.1358	34390	297.1306	15510
265.1407	30880	281.1727	3520	297.1689	3455
265.1786	2511	282.1388	3130	298.1326	2078
266.109	2779	283.1162	14310	299.1126	2857
266.1453	2132	283.1514	5518	299.1489	2546
267.0852	6936	285.0984	2003	301.1394	3521
267.1205	42130	285.132	3084	303.1219	4053
267.1567	7323	287.125	2806	303.1562	7834
268.1221	3450	289.1037	2097	305.0993	2024

Table A10. High Resolution Mass Spectra of GA before irradiation (*cont.*)

Mass	Intensity	Mass	Intensity	Mass	Intensity
305.1368	25310	323.1094	3579	345.1672	5507
305.1724	8367	323.1471	37530	347.1481	7743
306.1391	2776	323.1848	5299	347.1823	8466
307.1156	11610	324.1517	2945	349.1245	2791
307.1511	31460	325.1278	9043	349.1627	19250
307.1876	4460	325.1602	9776	349.1981	6204
308.1223	2182	327.1438	4805	351.1432	10720
308.1561	2416	331.153	5588	351.1774	13660
309.1323	30640	331.1862	3135	353.1573	9610
309.1669	13890	333.1308	5429	353.1933	3277
310.1335	2951	333.1661	14150	355.1379	2465
311.1119	5787	333.2045	2263	355.1765	2843
311.1459	14720	335.1479	19130	359.1516	2827
313.1284	4636	335.1812	12730	359.1809	4271
315.1551	2240	336.1525	2160	361.1638	9176
317.1382	5475	337.1274	8008	361.1988	4784
317.171	4445	337.1618	21260	363.1418	5421
319.1159	3613	337.199	3066	363.1771	14830
319.1524	16930	338.1654	2399	363.2141	3304
319.1874	5105	339.1434	11810	365.1583	12390
320.1547	2048	339.1785	4762	365.1929	8829
321.1328	20550	341.1572	10320	367.1369	2749
321.1661	22540	343.1491	2151	367.1725	7610
322.1329	2273	345.1317	2003	369.1539	3300

Table A10. High Resolution Mass Spectra of GA before irradiation (*cont.*)

Mass	Intensity	Mass	Intensity	Mass	Intensity
369.1904	2256	397.1848	3837	433.1863	3148
371.1799	2428	401.1939	3068	433.22	6141
373.1624	3415	403.1714	3734	435.2006	6125
373.1968	3070	403.2078	5317	435.2362	2608
375.1775	8523	405.1899	10030	437.1748	2079
375.2136	3215	405.2256	3700	437.2137	4282
377.1571	6450	407.171	5084	439.1985	2659
377.1935	11090	407.2044	6657	441.213	2202
379.1743	12050	409.1852	5980	443.2028	2343
379.2109	4098	409.2178	2520	445.2173	4210
381.1513	3996	411.1628	2305	447.1972	3894
381.1878	5168	415.2079	2956	447.2366	3589
383.1712	3070	417.1895	4491	449.2136	5376
387.1792	3671	417.2267	3377	451.19	2797
387.2122	2184	419.1662	2359	451.2289	3712
389.1544	2664	419.2049	7604	453.2078	2652
389.1918	7784	419.2435	2153	459.1967	2448
391.1742	9772	421.186	6924	459.2353	3491
391.2085	7390	421.2206	4541	461.2154	3614
393.1505	3244	423.1598	2011	461.2526	2693
393.1884	11080	423.1989	5910	463.1935	3145
393.2271	2417	425.1814	2669	463.2323	3509
395.1692	6195	429.1844	2002	465.2103	2832
395.2048	3591	431.2039	5158	465.241	2242

Table A10. High Resolution Mass Spectra of GA before irradiation (*cont.*)

Mass	Intensity
471.2326	2066
473.2161	2805
475.2283	4345
477.2098	3687
477.2509	3131
479.2237	3318
487.2329	2707
489.2459	2060
491.2283	3100
493.2397	2029
495.2251	2207
501.2342	3124
503.2418	4813
505.2438	2824
517.2421	2388
519.2604	2156
531.2468	2762
535.2487	2121
545.2705	2078
549.2678	2339
573.2626	2099
599.2955	2049
603.2866	2342

Table A11. Concentration of GA (μM) for photocatalytic experiment on effect of photocatalyst concentration

Sample		Time (min)								
		0	15	30	45	60	75	90	105	120
Photolysis		102.36	100.40	101.65	101.16	106.56	105.30	-	-	-
Catalysis		95.68	96.59	90.91	93.83	96.27	90.39	-	-	-
2 g/L	R1	107.99	98.48	84.17	69.03	59.88	52.26	-	-	-
	R2	98.15	91.86	77.35	69.94	64.24	59.16	-	-	-
	R3	102.61	89.63	72.36	59.42	57.13	56.05	-	-	-
	Avg	102.92	93.32	77.96	66.13	60.42	55.82	-	-	-
	SD	4.93	4.61	5.93	5.83	3.58	3.46	-	-	-
5 g/L	R1	98.70	67.84	42.31	25.19	14.71	8.82	5.92	3.87	3.24
	R2	89.64	58.46	33.70	18.50	12.18	9.12	6.74	5.47	4.34
	R3	93.17	61.46	37.45	28.97	16.27	11.96	7.39	6.30	5.10
	Avg	93.84	62.59	37.82	24.22	14.39	9.97	6.68	5.21	4.23
	SD	4.57	4.79	4.31	5.30	2.06	1.73	0.73	1.23	0.93
8 g/L	R1	89.74	54.60	26.75	12.03	5.51	2.75	-	-	-
	R2	96.00	66.08	31.25	17.60	8.72	4.09	-	-	-
	R3	99.69	47.99	21.04	12.15	5.03	3.01	-	-	-
	Avg	95.14	56.22	26.34	13.93	6.42	3.28	-	-	-
	SD	5.03	9.15	5.12	3.18	2.00	0.71	-	-	-

Table A12. Concentration of GA (μM) for photocatalytic experiment on effect of pH

Sample		Time (min)					
		0	15	30	45	60	75
pH 5	R1	102.08	99.75	96.94	94.79	94.23	93.47
	R2	89.59	87.46	85.29	84.14	83.45	82.45
	R3	97.99	95.22	91.95	90.32	89.44	88.46
	Avg	96.55	94.14	91.39	89.75	89.04	88.13
	SD	6.37	6.22	5.85	5.34	5.40	5.52
pH 6	R1	99.22	89.63	74.94	54.46	43.54	39.32
	R2	102.12	96.65	75.09	59.34	46.50	32.99
	R3	97.12	79.82	69.64	62.84	57.37	52.26
	Avg	99.49	88.70	73.22	58.88	49.14	41.52
	SD	2.51	8.45	3.11	4.21	7.28	9.82
pH 7	R1	98.70	67.84	42.31	25.19	14.71	8.82
	R2	89.64	58.46	33.70	18.50	12.18	9.12
	R3	93.17	61.46	37.45	28.97	16.27	11.96
	Avg	93.84	62.59	37.82	24.22	14.39	9.97
	SD	4.57	4.79	4.31	5.30	2.06	1.73
pH 8	R1	93.30	56.85	28.69	15.92	8.16	3.97
	R2	92.07	60.14	32.82	17.73	8.63	4.33
	R3	95.44	68.59	41.21	25.13	14.97	6.20
	Avg	93.60	61.86	34.24	19.60	10.59	4.84
	SD	1.71	6.05	6.38	4.88	3.80	1.20
pH 9	R1	97.73	50.56	31.65	16.61	7.98	4.01
	R2	99.75	62.40	35.28	16.42	7.15	3.72
	R3	94.20	52.01	24.78	12.08	5.64	2.80
	Avg	97.23	54.99	30.57	15.04	6.92	3.51
	SD	2.81	6.46	5.33	2.57	1.18	0.63

Table A13. Concentration of GA (μM) for photocatalytic experiment on effect of salt concentration

Sample		Time (min)					
		0	15	30	45	60	75
NaCl 0	R1	91.89	50.82	32.10	12.88	10.75	4.34
	R2	100.32	57.92	30.44	16.24	9.10	4.98
	R3	99.50	55.68	35.85	14.66	7.96	4.32
	Avg	97.24	54.81	32.80	14.60	9.27	4.55
	SD	4.65	3.63	2.77	1.68	1.40	0.37
NaCl 100	R1	95.09	54.17	37.08	21.22	13.54	7.35
	R2	91.79	52.75	33.68	19.61	11.60	7.34
	R3	98.01	67.21	39.18	23.82	14.99	6.09
	Avg	94.96	58.04	36.65	21.55	13.38	6.93
	SD	3.11	7.97	2.77	2.12	1.70	0.73
NaCl 200	R1	98.70	67.84	42.31	25.19	14.71	8.82
	R2	89.64	58.46	33.70	18.50	12.18	9.12
	R3	93.17	61.46	37.45	28.97	16.27	11.96
	Avg	93.84	62.59	37.82	24.22	14.39	9.97
	SD	4.57	4.79	4.31	5.30	2.06	1.73
NaCl 250	R1	91.06	77.14	46.32	35.08	23.90	17.72
	R2	103.02	84.96	70.89	59.65	41.20	27.92
	R3	93.84	77.85	63.37	53.67	40.06	27.40
	Avg	95.97	79.98	60.19	49.47	35.05	24.35
	SD	6.26	4.33	12.59	12.82	9.68	5.74
NaCl 300	R1	91.00	97.39	90.20	89.74	89.85	96.06
	R2	98.61	100.43	102.67	102.67	108.39	105.67
	R3	92.55	96.65	94.05	93.81	96.55	98.44
	Avg	94.05	98.16	95.64	95.41	98.26	100.06
	SD	4.02	2.00	6.38	6.61	9.39	5.00

Table A14. Concentration of GA (μM) for photocatalytic experiment on effect of GA initial concentration

Sample		Time (min)					
		0	15	30	45	60	75
400 μM	R1	353.48	323.30	312.18	276.12	246.26	220.53
	R2	371.76	331.47	302.66	254.39	227.79	199.88
	R3	375.12	335.48	317.88	271.51	253.70	228.98
	Avg	366.79	330.08	310.91	267.34	242.58	216.46
	SD	11.65	6.21	7.69	11.45	13.34	14.97
200 μM	R1	200.22	166.42	120.58	101.30	79.39	63.88
	R2	176.74	159.59	118.97	84.71	76.56	62.12
	R3	190.64	163.41	127.20	91.20	79.88	60.22
	Avg	189.20	163.14	122.25	92.40	78.61	62.07
	SD	11.81	3.42	4.36	8.36	1.79	1.83
100 μM	R1	98.70	67.84	42.31	25.19	14.71	8.82
	R2	89.64	58.46	33.70	18.50	12.18	9.12
	R3	93.17	61.46	37.45	28.97	16.27	11.96
	Avg	93.84	62.59	37.82	24.22	14.39	9.97
	SD	4.57	4.79	4.31	5.30	2.06	1.73

Table A15. Concentration of GA (μM) for photocatalytic experiment on effect of light source

Sample		Time (min)								
		0	15	30	45	60	75	90	105	120
Sunlight photolysis		94.19	95.76	91.41	88.92	96.69	97.06	89.37	92.28	92.24
350 nm	R1	97.33	33.19	7.95	2.16	0.66	-	-	-	-
	R2	90.80	33.12	9.72	3.73	1.04	-	-	-	-
	R3	89.69	33.64	11.15	3.37	1.11	-	-	-	-
	Avg	92.61	33.32	9.61	3.08	0.94	-	-	-	-
	SD	4.13	0.28	1.60	0.82	0.25	-	-	-	-
420 nm	R1	98.70	67.84	42.31	25.19	14.71	8.82	5.92	3.87	3.24
	R2	89.64	58.46	33.70	18.50	12.18	9.12	6.74	5.47	4.34
	R3	93.17	61.46	37.45	28.97	16.27	11.96	7.39	6.30	5.10
	Avg	93.84	62.59	37.82	24.22	14.39	9.97	6.68	5.21	4.23
	SD	4.57	4.79	4.31	5.30	2.06	1.73	0.73	1.23	0.93
Sunlight	R1	97.77	55.93	29.81	19.04	14.32	8.64	4.64	3.52	2.58
	R2	99.50	52.88	34.08	20.13	14.23	8.68	4.70	3.30	2.77
	R3	92.90	64.04	35.32	18.62	12.41	7.03	3.79	2.49	2.05
	Avg	96.72	57.62	33.07	19.26	13.65	8.12	4.38	3.10	2.46
	SD	3.42	5.77	2.89	0.78	1.08	0.94	0.51	0.54	0.38

Table A16. Concentration of GA (μM) for photocatalytic experiment on effect of quenchers

Sample		Time (min)	
		0	60
No Quencher	R1	98.70	8.82
	R2	89.64	9.12
	R3	93.17	11.96
	Avg	93.84	9.97
	SD	4.57	1.73
IPA	R1	111.33	28.45
	R2	105.92	25.53
	R3	104.56	25.96
	Avg	107.27	26.65
	SD	3.58	1.58
BQ	R1	99.15	74.51
	R2	100.81	74.02
	R3	102.44	76.23
	Avg	100.80	74.92
	SD	1.65	1.16
TEOA	R1	95.04	84.17
	R2	101.10	88.32
	R3	105.43	90.20
	Avg	100.52	87.56
	SD	5.22	3.08

VITA

Soklida Hong obtained his B.S. in Agricultural Science from Royal University of Agriculture, Cambodia, 2012. In 2013, He joined Chulalongkorn University, Thailand as an M.S. student in Environmental Management. In 2014, he joined Environmental and Conservation Sciences program at North Dakota State University as an M.S. student. Currently, his research is focused on photolysis and photocatalysis of glutaraldehyde in flowback and produced waters generated from unconventional oil production.